Spring 5-1-2024

COASTAL-OCEAN AND ESTUARINE ACIDIFICATION IN LONG BAY, SOUTH CAROLINA: A COMPARISON OF IN-SITU WATER QUALITY MONITORING WITH MEASURED CARBONATE SYSTEM PARAMETERS

Mary Olsen
Coastal Carolina University

COASTAL-OCEAN AND ESTUARINE ACIDIFICATION IN LONG BAY, SOUTH CAROLINA: A COMPARISON OF *IN-SITU* WATER QUALITY MONITORING WITH MEASURED CARBONATE SYSTEM PARAMETERS

By
Mary E. Olsen

A Thesis submitted
in Partial Fulfillment of the Requirements for the
Degree of Master of Science in
Coastal Marine and Wetland Studies

Gupta College of Science

Coastal Carolina University

2024

Dr. Angelos Hannides
Graduate Faculty Advisor, Coastal Carolina Univ.

Dr. Susan Libes
Committee Member, Coastal Carolina Univ.

Dr. April N. Abbott
Committee Member, Coastal Carolina Univ.

Mrs. Danielle Viso
Committee Member, Coastal Carolina Univ.

Mrs. Victoria Green
Committee Member, Coastal Carolina Univ.

Dr. Janet J. Reimer
Committee Member, Mid-Atlantic Regional Council on the Ocean

Dr. Emily R. Hall
Committee Member, Mote Marine Laboratory

Dr. Zhixiong Shen
MSCI Associate Chair of Graduate Programs

Dr. Chad Leverette
Dean, Gupta College of Science

Acknowledgements

First and foremost, I would like to thank my advisor Dr. Angelos Hannides for his endless support and guidance throughout my time at CCU. When I started working with him as an undergraduate, I never would have imagined that I would be where I am today. He has helped me become a confident scientist and has taught me so much along the way. With his guidance I have obtained knowledge, skills and relationships that will support me throughout my entire scientific career. I wouldn't be the scientist I am today without his continued support. Thank you for always being there for me.

I would also like to thank my committee members: Danielle Viso, Dr. April Abbott, Dr. Emily Hall, Dr. Susan Libes, Dr. Janet Reimer and Victoria Green, for their help and guidance throughout this project. I would also like to thank Jessica Frankle and Jaci Martinez from Mote Marine Laboratory for analyzing our samples and supporting me in any questions I had along the way. I would like to thank Abigial Caviris with her continued help in sample collection and sensor maintenance as well as other graduate students and scientists that helped me learn and grow through other perspectives including: Sarah Wessinger, Zach Czoer, Grace Kahmann, Zeke Meyers, Meredith Pfennig, Christina Maddox and Winter Widdifield.

I would like to thank South Carolina Sea Grant Consortium for funding this research, and the Southeast Ocean and Coastal Acidification Network, Mote Marine Laboratory, Environmental Quality Lab, Waccamaw Watershed Academy and Coastal Carolina University for their collaboration on this project. Monitoring at our two pier

stations is conducted with funding from Horry County (Apache Pier) and the City of North Myrtle Beach (Cherry Grove Pier), while the Murrells Inlet Volunteer Monitoring Program is funded by the Town of Surfside Beach, Georgetown County, and Horry County.

Finally, I want to thank my fiancé Marshall and my family for their unwavering support.

Abstract

One of the major water-quality issues impacting our coast and estuaries is coastal-ocean and estuarine acidification. Due to a relative dearth of data in the southeastern United States it is increasingly difficult to determine the full extent and intensity of this problem. This study provides the first characterization of coastal-ocean and estuarine acidification in Long Bay, SC by attempting to leverage long-term water quality data sets at two coastal-ocean pier sites using *in-situ* YSI EXO sondes deployed at both the surface and bottom waters along with two estuarine sites sampled by volunteer monitors using Orion star multi-meters. Discrete samples (120) for Dissolved Inorganic Carbon (DIC) and Total Alkalinity (TA) were collected from July 2022 to February 2023 contemporaneously to current routine observations at our four sites using the methods of Reimer et al. (2017). DIC and TA were measured according to Wang and Cai (2004). CO2SYS was used to calculate pCO_2, free $[H^+]$, pH_T, Ω_{CA} and Ω_{AR}. Property-property plots (pH_{NBS} vs. pH_T, TA vs. Salinity and pH_T vs. Salinity, Temperature and Dissolved Oxygen) were compared using geometric mean regression. Sensor pH_{NBS} measurements were compared to calculated pH_T measurements. Data show that DIC and TA peaks coincide with Chl a increases and DO decreases which indicates respiration taking place and adding CO_2 into the system (Schulz and Riebesell 2013). Oyster Landing and Rum Gully Creek both had values that fell within the pH_T, pCO_2, Ω_{CA} and Ω_{AR} thresholds for

Eastern Oysters (Gobler and Talmage 2014) and Summer Flounder (Chambers et al. 2014) indicating periodic events where they could be experiencing acidification events detrimental to their development. The estuarine sites showed strong linearity at Oyster Landing and Rum Gully Creek. No strong linear relationships were found between TA and salinity due to a highly dynamic coastal system. Current methodologies used by the volunteer monitoring program, at the estuarine sites, shows pH_{NBS} can potentially act as a proxy for pH_T. However, due to the lack of a conservative relationship between TA and salinity more information is needed to identify potential acidification trends. Future studies should be done to obtain more observations and sampling to better identify potential acidification trends (Pimenta and Grear 2018). Due to the highly dynamic nature of these systems future sampling should also include measuring pH_T from discrete samples in the laboratory to compare CO2SYS calculated pH_T to the discretely measured pH_T to help identify areas of error (Dickson et al. 2007, Fassbender et al. 2017). There should be a future focus on the need for better and more holistic data collection (i.e. nutrients, carbonate parameters, water quality parameters, etc.) in order to better understand and describe potential acidification in these estuarine and coastal-ocean systems.

Table of Contents

List of Tables

List of Figures

List of Symbols and Abbreviations

ABW	Apache Pier Bottom Water
$\hat{A}_i$	Modeled nTA
A_i	Calculated nTA
ASW	Apache Pier Surface Water
b	Y-intercept
BOD	Biological Oxygen Demand
C	Calcification
Ca^{2+}	Calcium
$CaCO_3$	Calcium Carbonate
CBW	Cherry Grove Pier Bottom Water
CD	Calcification and Dissolution
C:N:P	Carbon:Nitrogen:Phosphorus ratio
CO_2	Carbon Dioxide
CO2SYS	Program developed for carbon dioxide system calculations

CO_3^{2-}	Carbonate
COA	Coastal-Ocean Acidification
CRM	Certified Reference Materials
CSW	Cherry Grove Pier Surface Water
D	Dissolution
DIC	Dissolved Inorganic Carbon
DO	Dissolved Oxygen
DOM	Dissolved Organic Matter
GMR	Geometric Mean Regression
H^+	Hydrogen
H_2O	Water
H_3PO_4	Phosphoric Acid
HCl	Hydrochloric Acid
HCO_3^-	Bicarbonate
HSO_4^-	Hydrogen bisulfate
H_2CO_3	Carbonic Acid
IUPAC	International Union of Pure and Applied Chemistry
K_S	Acid dissociation constant for HSO_4^-

K_{spx}	Solubility constant for aragonite
LBHMC	Long Bay Hypoxia Monitoring Consortium
m	Slope
MML	Mote Marine Laboratory
n	Sample size
NBS	National Bureau of Standards
NCC	Net Community Calcification
NCP	Net Community Production
nDIC	Salinity normalized dissolved inorganic carbon
nTA	Salinity normalized total alkalinity
OA	Ocean Acidification
OM	Organic Matter
OYL	Oyster Landing
P =	P-value
P	Photosynthesis
$\bar{P}$	Mean pH_{NBS}
$\hat{P}_i$	Modeled pH_{NBS}
pCO_2	Partial Pressure of carbon dioxide

PD	Photosynthesis and Dissolution
pH_F	Free hydrogen scale
pH_{NBS}	National Bureau of Standards scale
pH_{SWS}	Seawater Scale
pH_T	Total hydrogen scale
P_i	Measured pH_{NBS}
PR	Photosynthesis and Respiration
R	Respiration
r	Correlation Coefficient
r^2	Coefficient of Determination
RC	Respiration and Calcification
RGC	Rum Gully Creek
SC	South Carolina
S_{NN}	Sum of squares of the residuals of measured pH_{NBS}
S_{mean}	Mean salinity
$S_{measured}$	Measured salinity
S_r	Least Squares Regression
S_T	Total Sulfate Concentration

S_{TT}	Sum of squares of the residuals of measured pH_T
[sign(r)]	The sign of the linear correlation coefficient
$\hat{T}_G$	GMR estimate of the line equation
$\bar{T}$	Mean pH_T
$\hat{T}_i$	Modeled pH_T
TA	Total Alkalinity
TA-org	Organic Alkalinity
T_i	Measured pH_T
WWA	Waccamaw Watershed Academy
α_G	Intercept
β_G	Slope
Ω	Saturation State
Ω_{AR}	Aragonite Saturation
Ω_{CA}	Calcite Saturation

Introduction

Ocean Acidification (OA)

Ocean acidification (OA) is the decrease in surface ocean pH due to oceanic uptake of atmospheric carbon dioxide (CO_2) (Duarte et al. 2013, Patsavas et al. 2015, Gledhill et al. 2015). The main stoichiometric reactions that control CO_2 speciation in water is shown by the reactions in Equation *1a-d* and Figure 1 (Dickson et al. 2007, Pimenta and Grear 2018, Feely et al. 2023):

$$CO_2(g) \leftrightarrow CO_2(aq) \qquad 1a)$$

$$CO_2^-(aq) + H_2O(l) \leftrightarrow H_2CO_3(aq) \leftrightarrow H^+(aq) + HCO_3^-(aq) \qquad 1b)$$

$$HCO_3^-(aq) \leftrightarrow H^+(aq) + CO_3^{2-}(aq) \qquad 1c)$$

$$CaCO_3 + CO_2 + H_2O \leftrightarrow Ca^{2+} + 2HCO_3^- \qquad 1d)$$

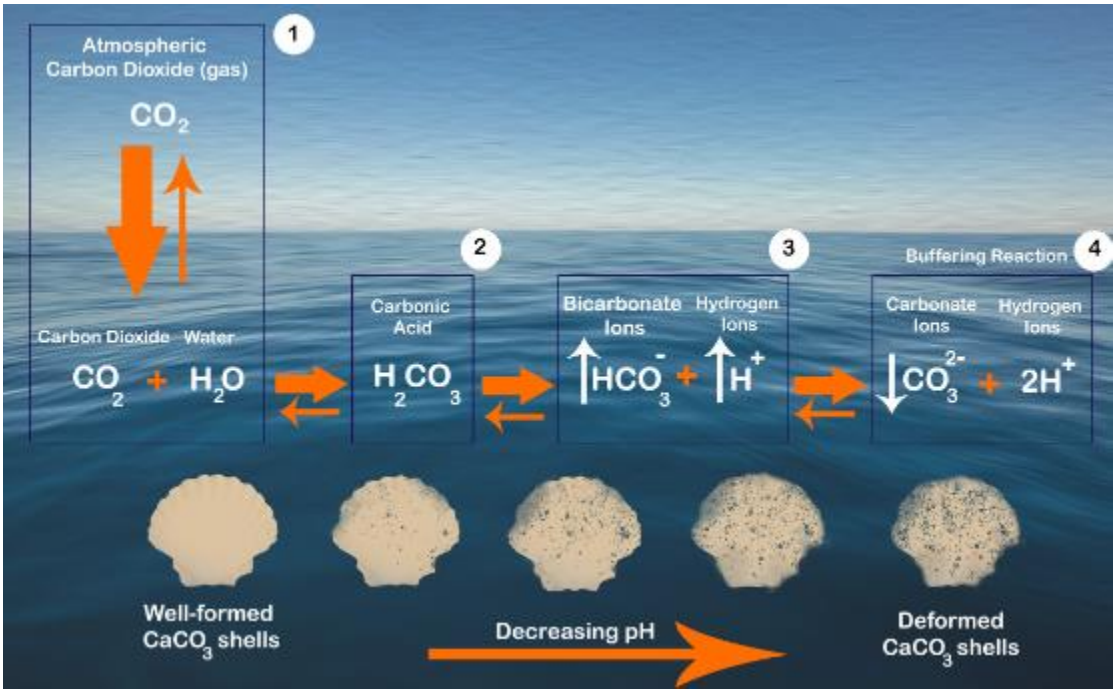

Figure 1. Graphic of the stoichiometric reactions that control CO_2 speciation in seawater leading to acidification. NOAA OAP (Jewett et al. 2020).

The air-sea exchange of CO_2 (*1a*) leads to an initial increase in dissolved CO_2 from gas exchange (Patsavas et al. 2015, Wanninkhof et al. 2015, Feely et al. 2018) (Figure 1). The ocean acts as a large reservoir for CO_2 and has currently absorbed about 31% of anthropogenic carbon emissions resulting in a significant decrease in oceanic pH (Hall et al. 2020, Reimer et al. 2017). With increasing CO_2 emissions, the open ocean's capacity to absorb anthropogenic CO_2 will decrease (Gattuso et al. 2015). The dissolved CO_2 reacts with water (H_2O) to form carbonic acid (H_2CO_3) which then dissociates into a hydrogen ion (H^+) and a bicarbonate ion (HCO_3^-) (*1b*) (Figure 1). Surface ocean acidity has increased by around 26% since 1860 causing a drop in pH from 8.2 to 8.1 (Tanhua et al. 2015, Feely et al. 2023). HCO_3^- can dissociate into a H^+ and a carbonate ion (CO_3^{2-})

(*1c*) (Figure 1). This is concerning for marine organisms, specifically calcifiers, since a reduction in available carbonate ions makes it more difficult to form biogenic calcium carbonate ($CaCO_3$) and requires more energy to be expended by these organisms (Guinotte and Fabry 2008). Additionally, dissolved calcium (Ca^{2+}) can combine with HCO_3^- to produce a $CaCO_3$ mineral (*1d*) such as aragonite or calcite. The addition of atmospheric CO_2 leads to overall increases in H^+ and HCO_3^- and decreases in CO_3^{2-} which decreases pH (Patsavas et al. 2015, Wanninkhof et al. 2015, Feely et al. 2018, Feely et al. 2023).

Carbonate Chemistry Parameters

The saturation states (Ω) of $CaCO_3$ minerals in seawater (i.e. aragonite (Ω_{AR}) and calcite (Ω_{CA})) are described by equation (*2a-b*).

$$\Omega_{AR} = \frac{[Ca^{2+}]_T[CO_3^{2-}]_T}{K_{spAR}} \qquad 2a)$$

$$\Omega_{CA} = \frac{[Ca^{2+}]_T[CO_3^{2-}]_T}{K_{spCA}} \qquad 2b)$$

The total concentrations of each species are represented by the brackets ($[\ ]_T$). $[Ca^{2+}]_T$ and $[CO_3^{2-}]_T$ are the concentrations of dissolved calcium and carbonate ions in seawater. K_{spAR} is the solubility product for aragonite and K_{spCA} is the solubility product for calcite. Marine organisms secrete calcium carbonate in the commonly found forms of aragonite and calcite (Röckstrom et al. 2009, Duarte et al. 2013). With rising ocean acidity, aragonite shells are expected to dissolve before those made of calcite due to

aragonite being about 50% more soluble in seawater than calcite (Röckstrom et al. 2009). Ω_{AR} in the Sargasso Sea at the Bermuda Atlantic Time-series site changed by -0.009 ± 0.001 per year since 1983 (Bates and Johnson 2023). The aragonite saturation horizon which is defined as the depth at which $\Omega_{AR} = 1$ is around 2200 – 2500m in the Atlantic Ocean (Jiang et al. 2015). Undersaturation is at $\Omega < 1$, however, detrimental effects on marine organisms have been documented well above the geochemical threshold of $\Omega = 1$. Therefore, Röckstrom et al. 2009 proposed a boundary for surface ocean aragonite saturation at $\Omega_{AR} = 2.75$. The global area averaged calcite saturation from 2015 cruises shows a level of $\Omega_{CA} = 4.54$ and this has decreased by -0.12 per decade since 1975 (Feely et al. 2023).

Dissolved inorganic carbon (DIC) is the sum of inorganic carbon species and mostly exists as carbonate and bicarbonate ions (Dickson et al. 2007, Pimenta and Grear 2018). It can be measured directly through acidifying the sample, removing the CO2 gas formed and measuring it with instruments including infrared, spectrophotometric and coulometric detection (Dickson et al. 2007, Pimenta and Grear 2018). DIC is defined by equation (*3*):

$$\text{DIC} = [CO_2^*] + [HCO_3^-]_T + [CO_3^{2-}]_T \qquad 3)$$

where CO_2^* is the sum of aqueous CO_2 and carbonic acid [H_2CO_3] (Patsavas et al. 2015).

Total alkalinity (TA) in the simplest definition is the excess of proton acceptors (bases formed from weak acids) over proton donors relative to a reference point (Dickson et al. 2007, Pimenta and Grear 2018). It is the ability of constituents in seawater to react with the addition of a strong acid and then transform it to an uncharged species (Pimenta and Grear 2018). In general, higher salinity waters will have higher alkalinity and a better capability to buffer acids. Organic alkalinity from dissolved organic matter contributes to TA in estuarine and coastal waters and can have a large effect on TA in the system (Fassbender et al. 2017, Pimenta and Grear 2018). Acidimetric titration using colorimetric or potentiometric methods can be used to measure TA (Gran 1952, Dickson et al. 2007, Pimenta and Grear 2018). TA is defined by equation (*4*):

$$\mathrm{TA} = [HCO_3^-]_T + 2[CO_3^{2-}]_T + [B(OH)_4^-]_T + [OH^-]_T + [HPO_4^{2-}]_T + 2[PO_4^{3-}]_T + [SiO(OH)_3^-]_T - [H^+]_T - [H_3PO_4^0] + [\text{organic bases}] \qquad 4)$$

The hydrogen ion concentration in seawater is normally represented by pH (Dickson et al 2007). Changes in pH reflect relative changes in $[H^+]$ rather than absolute changes. Total hydrogen ion concentration is defined by equation (*5*)

$$[H^+]_T = [H^+]_F\left(1 + \frac{S_T}{K_S}\right) \qquad 5)$$

$[H^+]_T$ is the total hydrogen ion concentration, $[H^+]_F$ is the free hydrogen ion concentration, S_T is the total sulfate concentration ($[SO_4^{2-}] + [HSO_4^-]$) and K_S is the acid dissociation constant for HSO_4^- (Dickson et al. 2007).

There are four pH scales commonly used in seawater pH measurements. The four scales are the National Bureau of Standards (NBS) also known as International Union of Pure and Applied Chemistry (IUPAC) scale (pH_{NBS}), seawater scale (pH_{SWS}), free hydrogen scale (pH_F) and total hydrogen scale (pH_T). In coastal, oceanic and estuarine systems the total hydrogen scale is the most appropriate to use because it includes the free hydrogen proton that dissociates from hydrogen bisulfate (HSO_4^-) which accounts for the high sulfate concentration in seawater (Pimenta and Grear 2018).

Total pH, pH_T, is the globally accepted pH observation for ocean acidification research (Patsavas et al. 2015) which measures the concentration of the free hydrogen ion along with the one that dissociates from hydrogen bisulfate (HSO_4^-) (Pimenta and Grear 2018). pH_T is defined by equation (*6*)

$$\mathrm{pH_T} = -\log[H^+]_T \qquad 6)$$

Most pH variations in the open ocean appear small since they are based on a logarithmic scale, but for a given pH change, the associated $[H^+]$ change varies depending on the initial $[H^+]$ concentration (Fassbender et al. 2021).

pCO_2 is the gas phase pressure of CO_2 which is in equilibrium with the dissolved carbon dioxide from the atmosphere. It can be calculated from any pairing combination of the carbonate parameters (TA, DIC and pH) along with the water temperature and salinity. The direct method for measuring pCO_2 uses gas chromatography or infra-red spectroscopy (Dickson et al. 2007, Pimenta and Grear 2018).

The CO_2 system in seawater is described by four measurable parameters including TA, DIC, pH and pCO_2. The measurement of any two of these parameters along with salinity, pressure, temperature and quantities of other components of seawater along with the appropriate equilibrium constants allows the calculation of the other two parameters not measured using CO2SYS, a program that performs carbonate system calculations (Lewis et al. 1998).

Coastal-Ocean and Estuarine Acidification (COA)

Coastal and estuarine waters represent crucial economic assets due to their richness in animal species and diverse natural habitats. Consequently, there is a growing focus on exploring the susceptibility of these waters to acidification due to the potential immediate effects on the health of the nearshore and estuarine ecosystems which in turn affects the local economies (Ekstrom et al. 2015, Gledhill et al. 2015 and Hu and Cai 2013).

Due to coastal regions being highly populated and urbanized, freshwater draining into coastal waterways transports large amounts of organic and inorganic nutrients, including nitrogen and phosphorus, to coastal waters (Flynn 2008). An increase in impervious surfaces prevents water from absorbing into the ground after rain events forcing the excess water to flow into rivers, estuaries and streams causing alterations in DO, salinity, temperature, and pH (Jartun et al. 2008). An increase in freshwater flow could lead to reduced carbonate ion concentrations and reduced buffering capacity in coastal waters (Salisbury et a. 2008, Cai et al. 2010, Hu and Cai 2013, Hall et al. 2020). In the U.S. Southeast, the carbonate chemistry of waters is greatly influenced by TA of

river water that discharges at the coast (Bauer et al. 2006, Cai et al. 2021) delivering poorly buffered waters that are high in pCO_2 (Cai et al. 2021). Transport of CO_2 rich water from estuaries is a crucial process that is contributing to coastal-ocean acidification (COA) (Reimer et al 2017, Hall et al. 2020).

Localized decreases in pH (Cai et al. 2011, Wallace et al. 2014, Pimenta and Grear 2018, Cai et al. 2021, Hall et al. 2024) are commonly due to increases in eutrophication, hypoxia and respiration that releases CO_2 (Bauer et al. 2006, Wang et al. 2016, Bates et al. 2014). Large nutrient inputs can cause eutrophication and when associated with vertical stratification in estuaries, this input can create large horizontal and vertical gradients in the carbonate system parameters, pH, and dissolved oxygen (DO) (Cai et al. 2021).

Hypoxia

Hypoxia, defined as depleted DO levels in the water column (< 2 mg/L or approximately 28% saturation) (Sanger et al. 2010), often accompanies elevated pCO_2 in coastal waters primarily resulting from oxygen consumption by respiration at night when photosynthesis declines and CO_2 fixation decreases (Cochran and Burnett 1996, Burnett 1997, Ianson et al. 2016). In stratified waters, respiration and remineralization can lead to hypoxia and have negative impacts on marine organisms (Wanninkhof et al. 2015). Aerobic respiration of organic matter consumes oxygen and produces CO_2 in approximate stoichiometric equivalence as shown in Equation 7 (Redfield et al. 1963, Feely et al. 2018):

$$(CH_2O)_{106}(NH_3)_{16}H_3PO_4 + 138O_2 \rightleftarrows 106CO_2 + 16HNO_3 + H_3PO_4 + 122H_2O \quad 7)$$

Coastal hypoxia has been increasing in frequency, duration and intensity globally over the last three decades and these low oxygen events can significantly alter biological communities in the water column (Sanger et al. 2010, Sanger et al. 2012). Since pCO_2-driven acidification can co-occur with hypoxia, as a consequence of coastal eutrophication and respiration, the combined effects of these two stressors could potentially be an enhanced threat to estuarine organisms (Cai et al. 2021).

OA vs. COA

OA is a global process that is mainly caused by atmospheric carbon dioxide entering the ocean causing a decrease in the pH of the ocean. COA is a more localized decrease in pH that is primarily caused by the release of carbon dioxide into the water from high levels of respiration, increased eutrophication and hypoxia (Pimenta and Grear 2018).

In the open ocean, pH is less variable with seasonal and diurnal deviations (Hofmann et al. 2011, Pimenta and Grear 2018) making open ocean trends easier to identify. Due to the open ocean's important role in the global carbon cycle more precise measurements have been taken of the carbon system for a much longer period of time which has allowed for a better understanding of OA. In the coastal-ocean however, there is much higher variability of pH which requires more samples and longer time-series to identify trends (Keller et al. 2014, Pimenta and Grear 2018). This poses a challenge for studying COA because the current

methodologies used to analyze samples for the carbonate system are expensive. This makes the extensive sampling needed to obtain high frequency and spatially robust data to identify spatial and time trends unreasonable due to financial limitations (Pimenta and Grear 2018).

Study Objectives

Long Bay is an open embayment located off the coasts of North and South Carolina (Sanger et al. 2012, Troup et al. 2017) that allows mixing of coastal and offshore waters. Consequently, extensive hypoxic events in this area would be unexpected, however, the coastlines of the Carolinas are highly urbanized and commercialized making their coastal waters extremely susceptible to hypoxia from increased nutrient inputs and eutrophication (Sanger et al. 2012, Troup et al. 2017). There is currently a lack of COA research on the coast of South Carolina (SC) and therefore this project aims to provide the first characterization of COA using decade-long data sets from Long Bay, SC where low pH and low oxygen (Sanger et al. 2012) have already been documented (Figure 2, Figure 3). This study aims to compare and validate historical long-term data for possible acidification events in the proposed region through discrete sampling of carbonate parameters (dissolved inorganic carbon [DIC] and total alkalinity [TA]) and the comparison to real-time water quality datasets. Measured versus calculated pH scales will be compared through internal consistency, the extent to which a measure yields the same value (Revicki 2014), to show that water quality parameters, as monitored by sensor technologies, can be used for COA assessment.

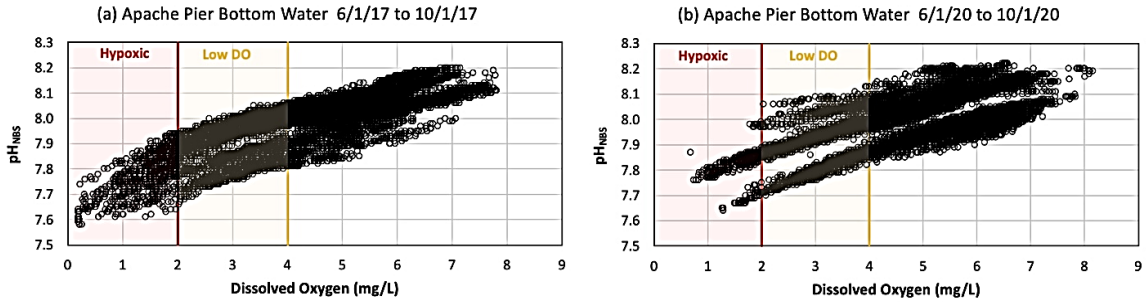

Figure 2. pH_{NBS} and DO (mg/L) from Apache Pier showing a positive correlation between the two parameters (Data source: LBHMC 2021; S. Libes, pers. comm.)

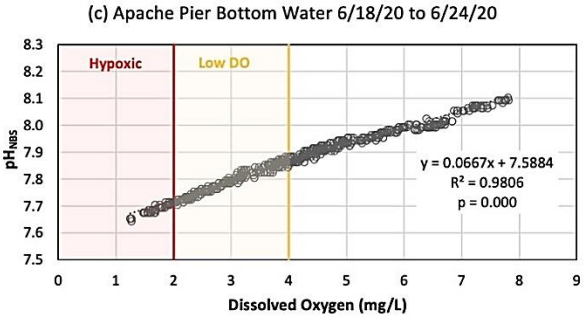

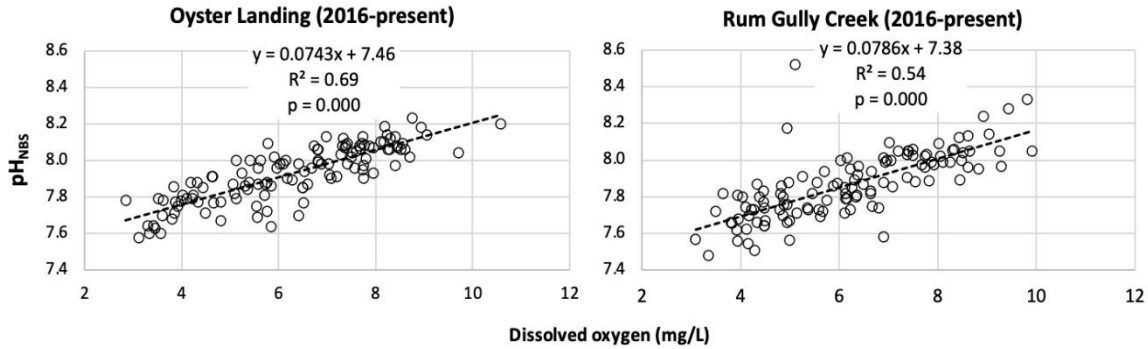

Figure 3. pH_{NBS} and DO (mg/L) from Oyster Landing and Rum Gully Creek showing a positive correlation between the two parameters (Data source: WWA 2021; S. Libes, pers. comm.).

Hypotheses

This study aims to address the following hypotheses:

1. The relatively low-accuracy but high temporal-frequency pH_{NBS} measurements that have been collected over the past decade at four sites in Long Bay, SC, can be used as a proxy for total-scale pH (pH_T), the globally accepted pH property for acidification monitoring.
    a. pH_{NBS} has a 1:1 relationship with $pH_{T.}$
2. Two coastal-ocean and two estuarine sites in Long Bay, SC have been experiencing decreasing pH and degree of saturation of calcite and aragonite over the past decade.
    a. Total Alkalinity has a direct relationship with salinity (in addition to 1a).
3. Estuarine sites are more prone to acidification than coastal-ocean sites.
4. pH at our study sites co-varies with temperature, dissolved oxygen and salinity.
    a. pH has an inverse relationship with temperature.
    b. pH has a direct relationship with dissolved oxygen.

c. pH co-varies with salinity.

Methods

Study Sites

Four sites were chosen for this project due to the presence of current water quality monitoring programs in Long Bay, SC (Table 1). The two coastal-ocean sites are located at Apache Pier, in Myrtle Beach, and Cherry Grove Pier, in North Myrtle Beach (Figure 4), where there are multiparameter YSI EXO sondes (YSI Incorporated, Yellow Springs, Ohio) that are collecting data in both the surface and bottom waters every 15 minutes since 2012 for pH_{NBS}, temperature, DO, salinity, turbidity, depth and chlorophyll (Data source: LBHMC 2021). The two sites in Murrells Inlet are located at Oyster Landing Beach (OYL) and Rum Gully Creek (RGC) (Figure 4) which are estuarine stations for a volunteer monitoring program (Libes et al. 2015) that has been sampling biweekly since 2008 for pH_{NBS}, temperature, DO, specific conductivity and salinity as well as other water quality parameters using Orion Star multimeters set in surface water grab samples (Thermo Fisher Scientific, Waltham, Massachusetts) (Data source: WWA 2021).

Table 1. Study site stations and corresponding instrumentation.

Station	**Acronym**	**Coordinates**	**Type**	**Platform**	**Sampling Frequency**	**Instrument-ation**
Apache Pier Bottom Water	ABW	33.76 -78.78	Coastal-ocean	*In-situ* deployed	15 minutes	YSI EXO sonde
Apache Pier Surface Water	ASW	33.76 -78.78	Coastal-ocean	*In-situ* deployed	15 minutes	YSI EXO sonde
Cherry Grove Pier Bottom Water	CBW	33.83 -78.63	Coastal-ocean	*In-situ* deployed	15 minutes	YSI EXO sonde
Cherry Grove Pier Surface Water	CSW	33.83 -78.63	Coastal-ocean	*In-situ* deployed	15 minutes	YSI EXO sonde
Oyster Landing	OYL	33.52 -79.06	Estuary	*In-situ* measure-ment	biweekly	Orion Star multimeters
Rum Gully Creek	RGC	33.57 -79.02	Estuary	*In-situ* measure-ment	biweekly	Orion Star multimeters

Figure 4. Study site and stations: (1) Segment of Long Bay, SC showing the study region; (a) Apache Pier (ABW and ASW), a coastal-ocean site, in Myrtle Beach, SC; (b) Cherry Grove Pier (CBW and CSW), a coastal-ocean site, in North Myrtle Beach, SC; (c) Oyster Landing (OYL), an estuarine site, in Murrells Inlet, SC; (d) Rum Gully Creek (RGC), an estuarine site, in Murrells Inlet, SC

Instrument pH Sensor (pH_{NBS}) Calibration and Post-Calibration Checks

Instrumentation for all sites measured pH on the NBS scale. The NBS scale measures hydrogen ion activity and is typically used by handheld meters and sondes (Pimenta and Grear 2018). The pH sensors of both the YSI EXO sondes and the Orion Star multimeters are calibrated and tested in-lab using NBS standards (Table 2). Deployed YSI EXO sondes are validated using the field check acceptance range (Table 2) during biweekly maintenance sessions using a recently in-lab calibrated instrument. Details are provided in Table 2.

Table 2. Instrument pH sensor calibration and post-calibration check details.

Stations	**Piers (coastal-ocean)**	**Volunteer Monitoring (estuary)**
Instrument	YSI EXO sondes	Orion Star multimeters
Manufacturer precision	±0.1 pH units within ±10°C of calibration temperature ±0.2 pH units for entire temperature range	0.01 pH units for entire temperature range. 0.03 pH units for buffers using automatic temperature compensation
Calibration standards (in-lab)	pH_{NBS}: 7.00,10.00	pH_{NBS}: 7.00,4.00
Post-calibration check standard (in-lab)	pH_{NBS}: 8.00	pH_{NBS}: 6.00
Post-calibration check (in-lab) acceptance range	±0.10	±0.10
Field check acceptance range	±0.20	±0.10

Field Sampling

Discrete water samples for DIC and TA were collected contemporaneously (time matched) to ongoing routine observations at our four sites using the methods of Reimer et al. (2017). A total of 120 discrete samples were collected from July 2022 to February 2023, including field replicates on every sampling event. We were only able to collect samples from Cherry Grove Pier (CBW and CSW) from July 2022 to September 2022 due to Hurricane Ian structurally damaging the pier and preventing further deployment and sampling. The rest of Cherry Grove's proposed samples were evenly distributed between the other sites. A Niskin bottle with tubing attached to prevent aeration of the samples, was used to collect water that was subsampled to fill 300-mL glass BOD bottles. Bottles were sealed with apiezon grease. Water was sampled at the corresponding depths associated with the site's instrumentation (Table 3). Samples were preserved with saturated mercuric chloride to prevent any biological activity that would impact the chemistry of the samples (e.g. photosynthesis and respiration). They were then stored on ice during transport from the field to the laboratory, where they were stored in a refrigerator until they were shipped to Mote Marine Laboratory in Sarasota, Florida for analysis.

Table 3. Niskin sampling depths (m) with ranges for the pier sites due variability in tidal changes. The estuarine sites (OYL and RGC) are sampled at a depth of 0.3m so they have no range.

Station	**Niskin sampling depth (m)**
ABW	5.2 – 7.0
ASW	1.1 – 1.4
CBW	4.2 – 6.0
CSW	1.1 – 1.3
OYL	0.3
RGC	0.3

Sample Analysis

DIC and TA samples were analyzed by the Ocean Acidification Program at Mote Marine Laboratory (MML). DIC was analyzed according to Wang and Cai (2004) using a nondispersive infrared laser LICOR analyzer after 1 ml of 10% H_3PO_4 was introduced into the sample and the CO_2 gas was "stripped" out. TA was measured via Gran titration with 0.05 N HCl to an end point of pH 3.2, also after Wang and Cai (2004). Accuracy was assessed with certified reference materials (CRMs) from the Dickson Laboratory at Scripps Institute of Oceanography. Precision for TA was 1.7 µmol/kg and for DIC was 1.6 µmol/kg. Accuracy was 2.5 µmol/kg for TA and 1.9 µmol/kg for DIC.

Carbonate Chemistry Characterization

The Microsoft Excel macro CO2SYS v.3.0 (Lewis et al. 1998, Pierrot et al. 2021) was used to calculate pCO_2, free $[H^+]$, pH_T, Ω_{CA} and Ω_{AR} using the DIC and TA results from the water sample analysis and the corresponding time-matched temperature, salinity and depth measurements from the YSI EXO sondes and the Orion Star multimeters. Settings used in the CO2SYS calculation are shown in Table 4 (Reimer et al. 2017). Equilibrium constants of Lueker et al. 2000 and boron constants from Lee et al. 2010 were used to give the closest match to the study sites.

Table 4. Settings selected for CO2SYS version 3.0 (Microsoft Excel macro) used in calculations.

Setting	**Selected option**
Set of Constants	K1, K2 from Lueker et al., 2000
$KHSO_4$	Dickson, 1990
KHF	Perez and Fraga, 1987
pH Scale	Total scale (mol/kg-SW)
$[B]_T$ Value	Lee et al., 2010
Temperature/Salinity	EOS-80

Data Analysis

Station Comparisons

Boxplots were used to show distributions at all six stations for each carbonate system parameter using MATLAB R2023a (MATLAB, 2023).

Statistical Methodology

A Kruskal-Wallis test was used to assess differences between means among the carbonate system parameters for all six sites due to the data being non-parametric using MATLAB R2023a (MATLAB, 2023).

nDIC vs. nTA

TA and DIC were normalized to salinity for nTA and nDIC:

$$nTA = TA * \left(\frac{S_{mean}}{S_{measured}}\right) \quad 8)$$

$$nDIC = DIC * \left(\frac{S_{mean}}{S_{measured}}\right) \quad 9)$$

where S_{mean} is the mean salinity from the samples and $S_{measured}$ is the salinity value from the corresponding measurement used to calculate TA and DIC. nTA-nDIC graphs were plotted using the approaches of Suzuki and Kawahata (2003), Muehllehner et al. (2016) and Hall et al. (2024). Theoretical lines representing the effects of photosynthesis (P), respiration (R), calcification (C) and dissolution (D) on nTA and nDIC were

calculated using the methods of Suzuki and Kawahata (2003) and Hall et al. (2024). The PR line is based on the Redfield ratio (Equation 7) for C:N:P of primary production for phytoplankton and the CD line is based on decreases in TA and DIC in a ratio of 2:1 (mole-to-mole) during calcification (Suzuki and Kawahata 2003, Hall et al. 2024). The upper right quadrant of each graph denotes net community respiration and net community carbonate dissolution as well as TA and DIC values greater than the mean values from the sampling period (Figure 26) (Hall et al. 2024). The lower left quadrant shows the net community production (NCP) and net community calcification (NCC) (Figure 26) (Hall et al. 2024).

Property vs. Property Relationships

Least squares regression (S_r) was used to examine the relationship between nTA and nDIC. S_r determines regression coefficients by minimizing the sum of squares of the residuals:

$$S_r = \sum_{i=1}^{n} (A_i - \hat{A}_i)^2 \qquad 10)$$

where $A_i$is the calculated nTA data (µmol/kg), $\hat{A}_i$ is the modeled nTA and n is the number of measurements.

Geometric Mean Regression (GMR) was used to test for the statistical significance of relationships between (1) pH_{NBS} and pH_T, (2) TA (µmol/kg) and Salinity (ppt), (3) pH_T and Salinity (ppt), and (4) Temperature (°C) and DO (mg/L). GMR is a

linear Model-2 regression that is the sum of the products of the residuals minimized for two dependent variables:

$$\sum_{i=1}^{n}\left(P_i - \widehat{P_i}\right)\left(T_i - \widehat{T_i}\right) = GMR \qquad 11)$$

where P_i is the measured pH_{NBS}, $\widehat{P_i}$ is the modeled pH_{NBS}, T_i is measured pH_T, $\widehat{T_i}$ is the modeled pH_T and n is the number of measurements.

The slope (β_G) and the intercept (α_G):

$$\widehat{\beta_G} = [sign(r)]\left(\frac{S_{TT}}{S_{NN}}\right)^{1/2} \qquad 12)$$

$$\widehat{\alpha_G} = \bar{T} - \widehat{\beta_G}\bar{P} \qquad 13)$$

where S_{TT} is the sum of squares of the residuals of the measured pH_T about the mean of the measured pH_T , S_{NN} is the sum of the squares of the residuals of the measured pH_{NBS} about the mean of the measured pH_{NBS}, [sign(r)] is the sign of the linear correlation coefficient, $\bar{T}$ is mean pH_T and $\bar{P}$ is mean pH_{NBS}.

The mathematical model of the GMR estimate of the line equation ($\widehat{T_G}$) is defined as:

$$\widehat{T_G} = \widehat{\alpha_G} + \widehat{\beta_G} P \qquad 14)$$

Results

In-situ Observations

In-situ discretely sampled observations from July 2022 to February 2023 at ABW, ASW, CBW, CSW, OYL and RGC shows water temperature (°C) decreasing over time and DO (mg/L) increasing over the full sampling period. pH_{NBS} changes alongside DO and drops after Hurricane Ian came through the area on September 30, 2022 (Figure 5, 6 and 7). Over the full COA sampling period water temperature ranged from 10 – 30 at ABW, ASW, OYL and RGC and from 25 – 30 at CBW and CSW (Figure 8). DO ranged from 4.5 – 9.3 at the coastal-ocean sites and from 3.9 – 8.4 estuarine sites (Figure 9). Salinity (ppt) ranged from 33.75 – 36.25 at coastal-ocean and from 27.29 – 35.99 at the estuarine sites (Figure 5, 6, 7 and 10). Salinity at the estuarine sites is slightly lower than the coastal-ocean pier sites (Figure 10). pH_{NBS} ranged from 7.93 – 8.21 at the coastal-ocean sites and from 7.62 – 8.16 at the estuarine sites (Figure 11).

In-situ measurements from the sensor readings from January 2022 to December 2023 show variable ranges. Temperature at all six stations ranged from 6 – 31 (Figure 8). DO at ABW and CBW ranged from 0.90 – 9.71, at ASW and CSW from 2.33 – 11.94

and at OYL and RGC from 3.23 – 9.42 (Figure 9). At the coastal-ocean pier sites, salinity ranged from 31.25 – 36.37 and at the estuarine sites, salinity ranged from 28.45 – 36.23 (Figure 10). pH_{NBS} ranged from 7.58 – 8.16 at the estuarine sites and at the coastal-ocean sites, pH_{NBS} ranged from 7.70 – 8.39 (Figure 11).

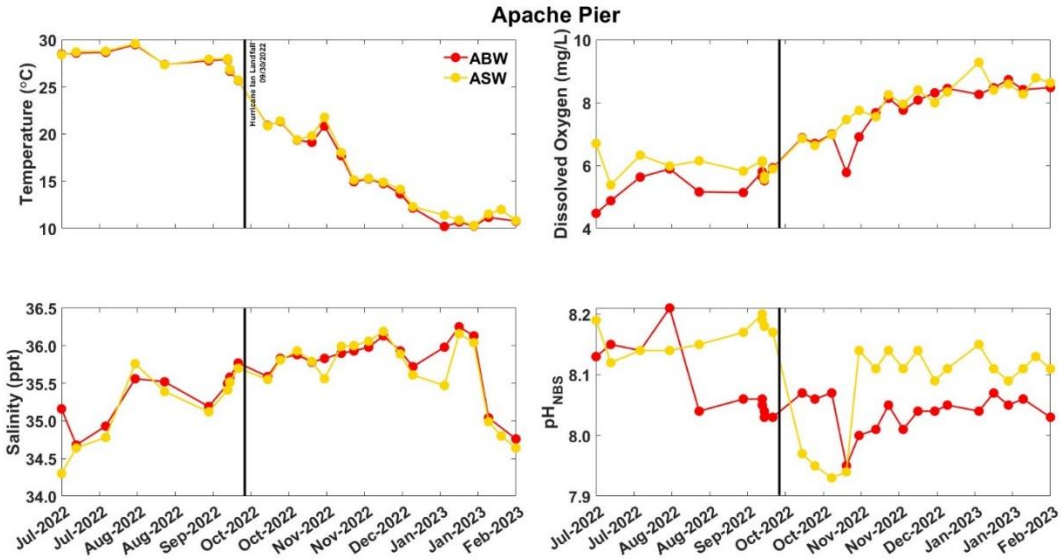

Figure 5. In-situ measurements from discrete sampling at Apache Pier from July 2022 to February 2023 (ABW:Bottom Water = red; ASW:Surface Water = yellow). Black vertical bars represent when Hurricane Ian made landfall on 9/30/2022. Diurnal sampling took place from September 22, 2022 at 20:30 to September 23, 2022 at 12:45.

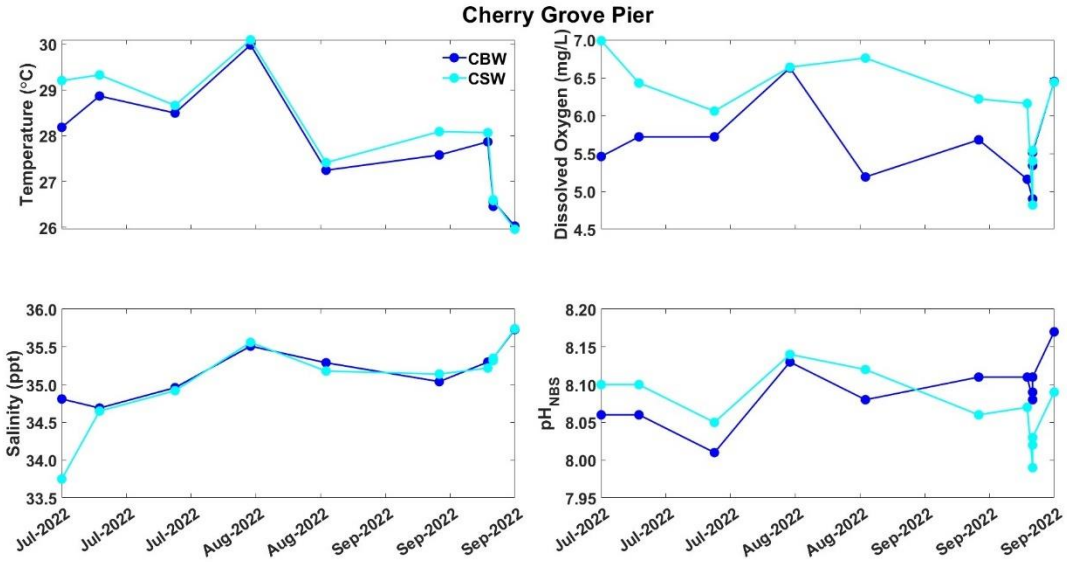

Figure 6. In-situ measurements at Cherry Grove Pier from July 2022 to September 2022 due to Hurricane Ian damage at the pier (CBW:Bottom Water = blue; CSW:Surface Water = cyan). Diurnal sampling took place from September 22, 2022 at 22:30 to September 23, 2022 at 10:30.

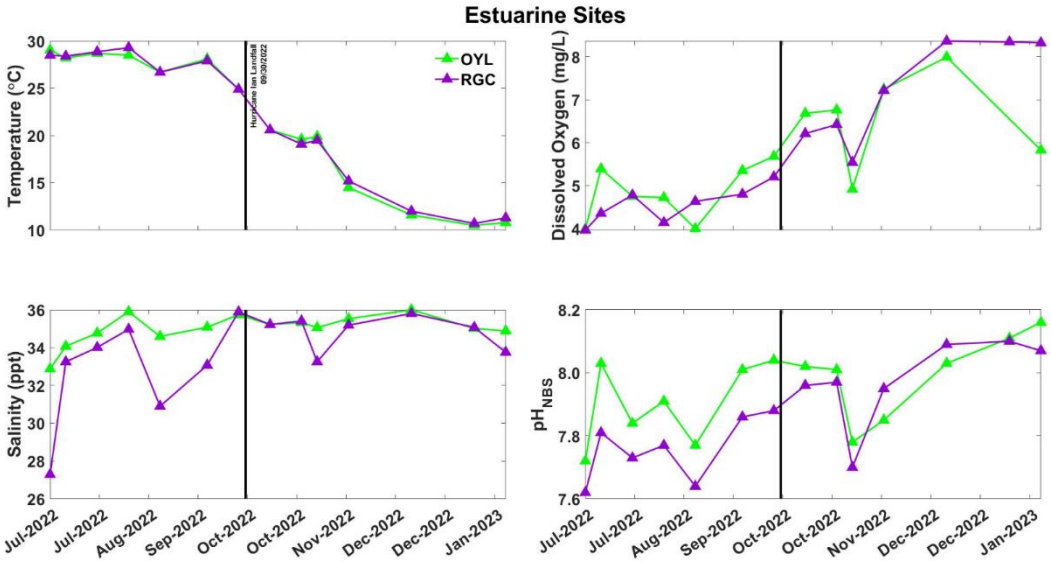

Figure 7. In-situ measurements at the Estuary sites from July 2022 to February 2023 (OYL:Oyster Landing = green; RGC:Rum Gully Creek = purple). Black vertical bars represent when Hurricane Ian made landfall on 9/30/2022.

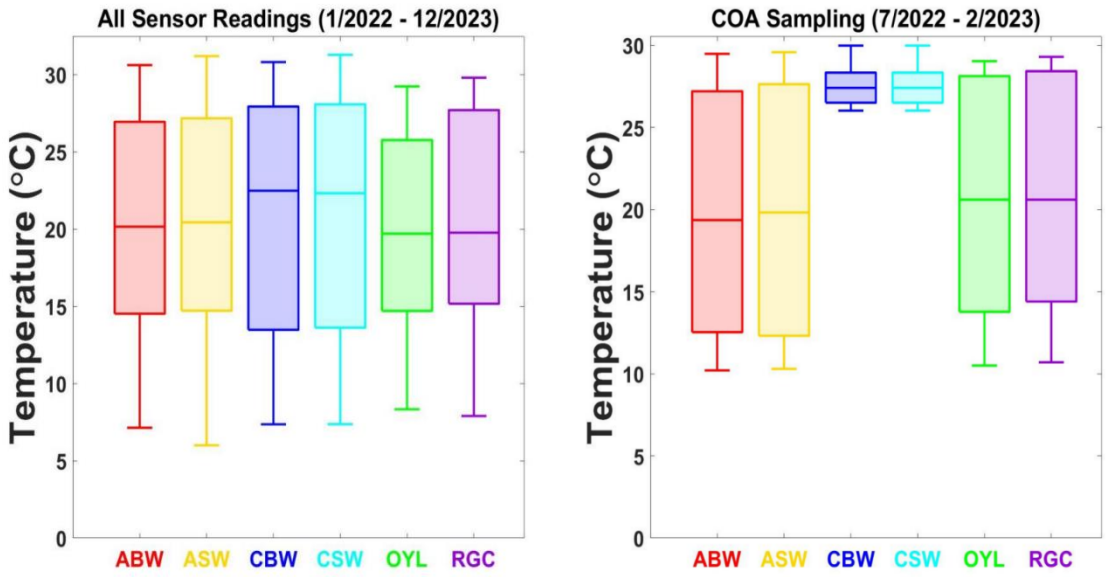

Figure 8. Boxplots of temperature ranges from sensor readings from January 2022 to December 2023 (left) (ABW: n = 69,247; ASW: n = 69,247; CBW: n = 66,265; CSW: n = 66,265; OYL: n= 46; RGC: n = 46) and sensor readings from COA sampling period from July 2022 to February 2023 (right) (ABW: n = 31; ASW: n = 32; CBW: n = 12; CSW: n = 11; OYL: n= 17; RGC: n = 17). Different colors represent site locations (ABW = red, ASW = yellow, CBW = blue, CSW = cyan, OYL = green, RGC = purple). Dots represent outliers which are data points more than 1.5 times the interquartile range away from the bottom or top of the box.

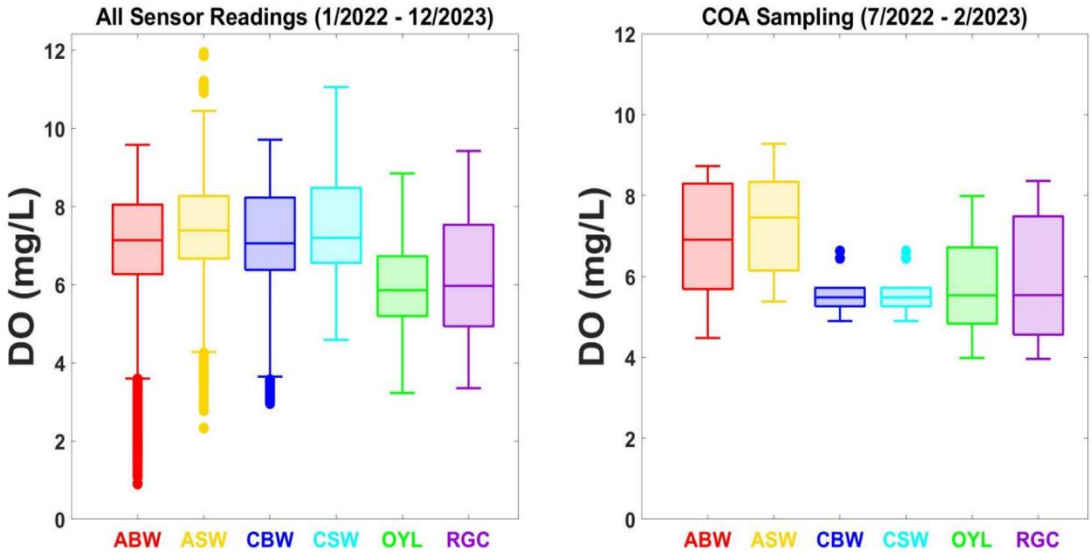

Figure 9. Boxplots of DO ranges from sensor readings from January 2022 to December 2023 (left) (ABW: n = 69,247; ASW: n = 69,247; CBW: n = 66,265; CSW: n = 66,265; OYL: n= 46; RGC: n = 46) and sensor readings from COA sampling period from July 2022 to February 2023 (right) (ABW: n = 31; ASW: n = 32; CBW: n = 12; CSW: n = 11; OYL: n= 17; RGC: n = 17). Different colors represent site locations (ABW = red, ASW = yellow, CBW = blue, CSW = cyan, OYL = green, RGC = purple). Dots represent outliers which are data points more than 1.5 times the interquartile range away from the bottom or top of the box.

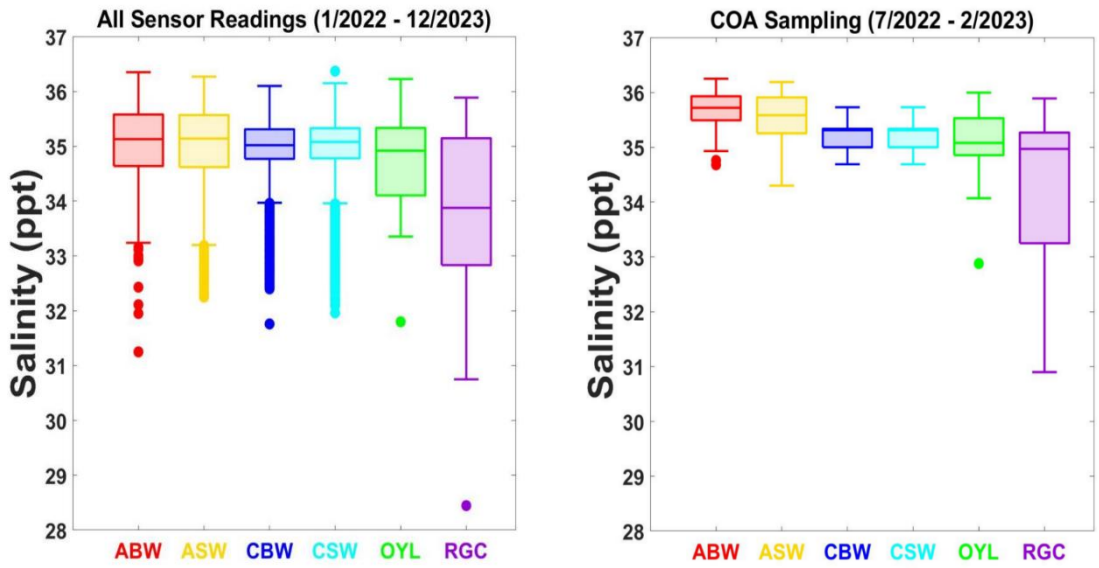

Figure 10. Boxplots of salinity ranges from sensor readings from January 2022 to December 2023 (left) (ABW: n = 69,247; ASW: n = 69,247; CBW: n = 66,265; CSW: n = 66,265; OYL: n= 46; RGC: n = 46) and sensor readings from COA sampling period from July 2022 to February 2023 (right) (ABW: n = 31; ASW: n = 32; CBW: n = 12; CSW: n = 11; OYL: n= 17; RGC: n = 17). Different colors represent site locations (ABW = red, ASW = yellow, CBW = blue, CSW = cyan, OYL = green, RGC = purple). Dots represent outliers which are data points more than 1.5 times the interquartile range away from the bottom or top of the box.

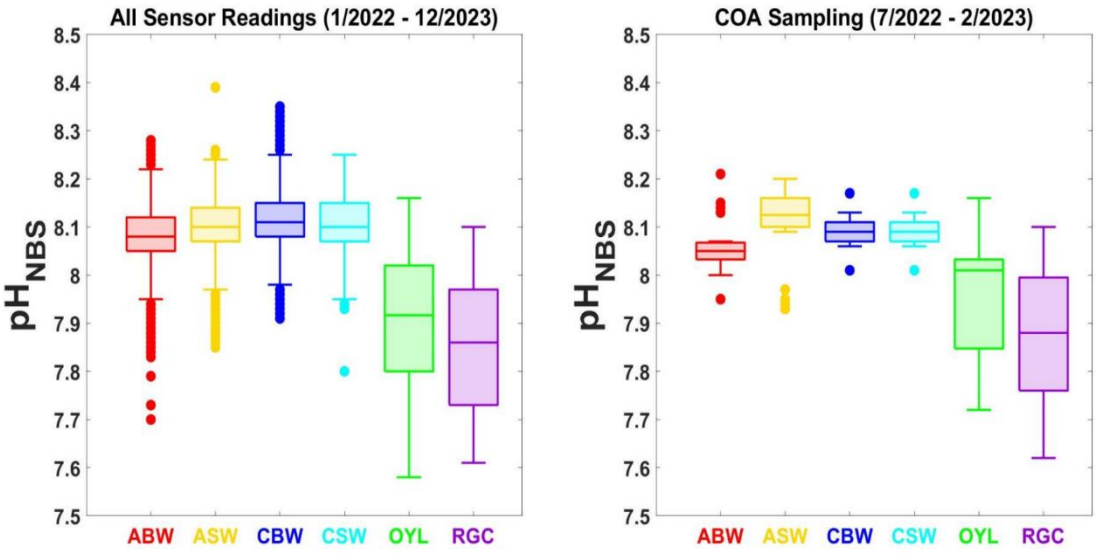

Figure 11. Boxplots of pH_{NBS} ranges from sensor readings from January 2022 to December 2023 (left) (ABW: n = 69,247; ASW: n = 69,247; CBW: n = 66,265; CSW: n = 66,265; OYL: n= 46; RGC: n = 46) and sensor readings from COA sampling period from July 2022 to February 2023 (right) (ABW: n = 31; ASW: n = 32; CBW: n = 12; CSW: n = 11; OYL: n= 17; RGC: n = 17). Different colors represent site locations (ABW = red, ASW = yellow, CBW = blue, CSW = cyan, OYL = green, RGC = purple). Dots represent outliers which are data points more than 1.5 times the interquartile range away from the bottom or top of the box.

Sample Analysis Results

TA (µmol/kg) and DIC (µmol/kg) at ABW, ASW, CBW, CSW, OYL and RGC shows similar trends between bottom water and surface water at the coastal-ocean sites and between the estuarine sites over the full sampling period (Figure 12, Figure 16, Figure 22). The estuarine sites have much larger ranges than the coastal-ocean sites for both TA and DIC (Figure 25). Extreme highs for TA at ABW occurred on November 1st and November 28th, 2022 while at ASW highs occurred just on November 28th, 2022 (Figure 12 and Figure 25). At OYL and RGC there are increases for both TA and DIC on November 1st, 2022. Extreme lows for DIC and TA at OYL and RGC occurred on July 12th and August 9th, 2022 (Figure 22). TA has multiple outliers for all the stations indicating these extrema points (Figure 25).

Diurnal sampling was performed at both coastal-ocean pier sites from September 22, 2022 at 20:30 to September 23, 2022 at 12:45 (Figure 15 and Figure 19). At Apache Pier for both TA and DIC, ABW and ASW have opposite patterns visually. ASW increases and ABW decreases between sampling points on September 22 in the evening (Figure 15). TA and DIC at Apache Pier on September 23 in the morning switch trends with ASW now decreasing and ABW increasing between sampling points (Figure 15). At Cherry Grove Pier for TA and DIC both CBW and CSW follow similar visual patterns with CBW and CSW increasing overnight (Figure 19). DIC for CBW and CSW decreases after high tide (Figure 19). TA for CBW decreases after high tide and increases for CSW (Figure 19). At both Apache and Cherry Grove Pier for the diurnal sampling, ABW and CBW were higher than ASW and ABW (Figure 15, Figure 19). Chlorophyll a (µg/L)

(Chl a) for ABW, ASW, CBW and CSW increase overnight (Figure 20) with corresponding decreases in DO (Figure 21). After sunrise DO increases (Figure 21) at all sites and chl a decreases with the incoming high tide (Figure 20).

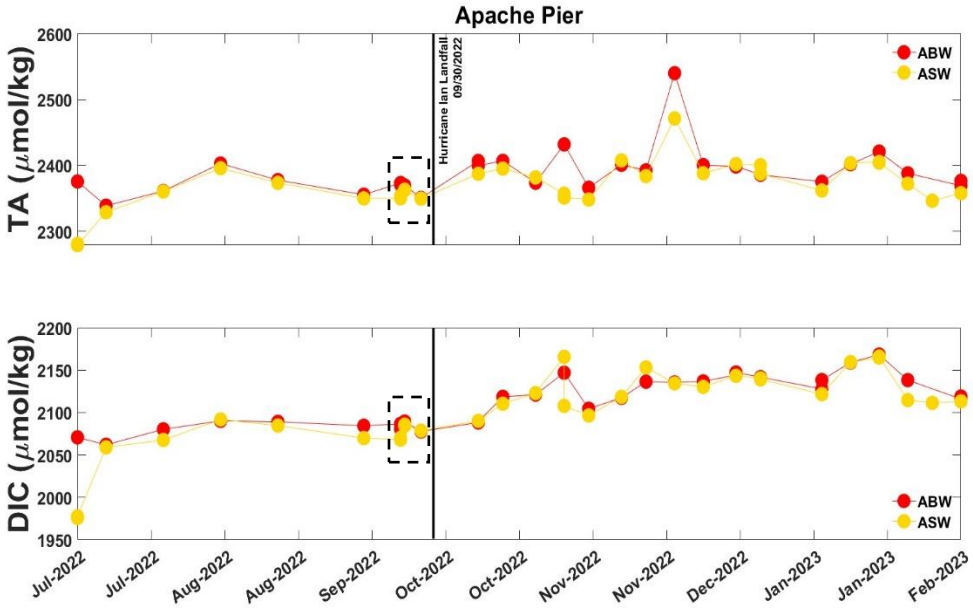

Figure 12. TA (μmol/kg) and DIC (μmol/kg) at Apache Pier from July 2022 to February 2023. Black vertical bars represent when Hurricane Ian made landfall on 9/30/2022. Error bars are smaller than the marker. Apache bottom water (ABW) = red and Apache surface water (ASW) = yellow. Black dashed boxes represent diurnal sampling zoomed in for Figure 15.

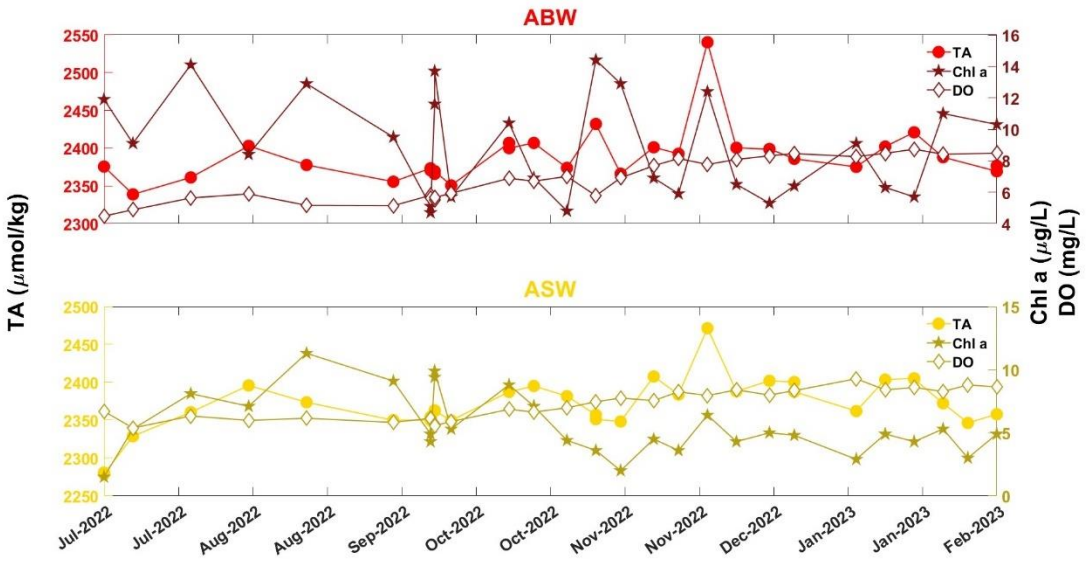

Figure 13. TA, Chl a and DO at Apache Pier (ABW and ASW) from the full sampling period (July 2022 to February 2023). TA = circles, Chl a = stars, DO = open diamonds.

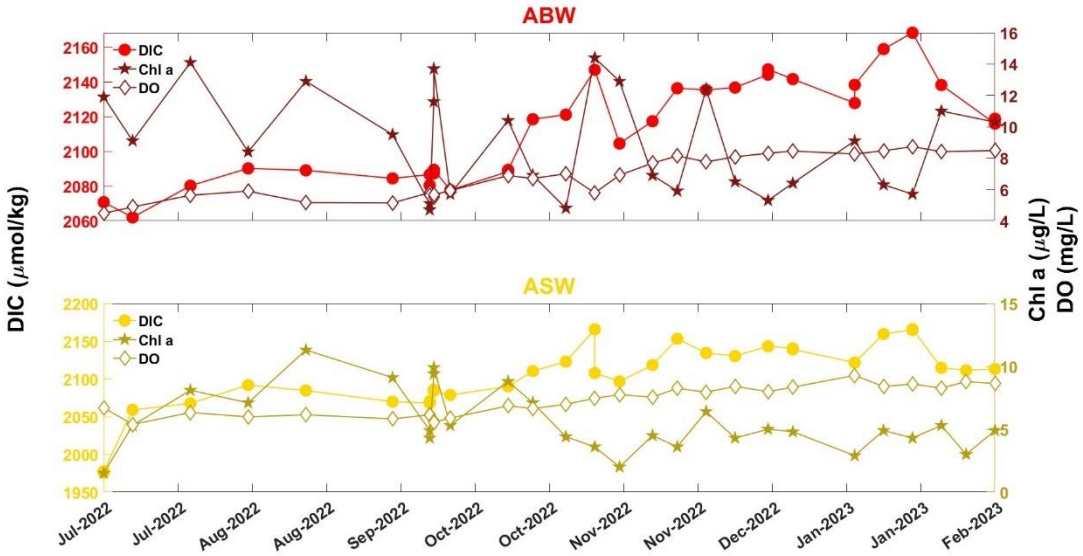

Figure 14. DIC, Chl a and DO at Apache Pier (ABW and ASW) from the full sampling period (July 2022 to February 2023). TA = circles, Chl a = stars, DO = open diamonds. Diurnal sampling took place from September 22, 2022 at 20:30 to September 23, 2022 at 12:45.

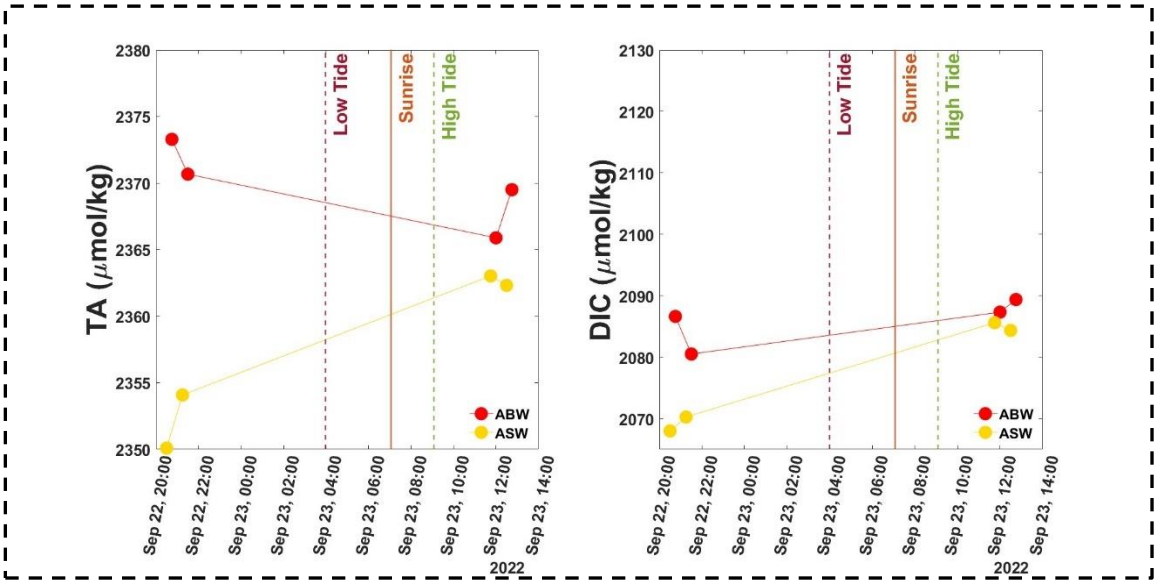

Figure 15. Diurnal pre-Hurricane Ian sampling for TA (μmol/kg) and DIC (μmol/kg) at Apache Pier. Sampling took place from September 22, 2022 at 20:30 to September 23, 2022 at 12:45. Lines represent low tide (dark red dashed line) at 03:59, high tide (green dashed line) at 09:05 and sunrise (orange solid line) at 07:04.

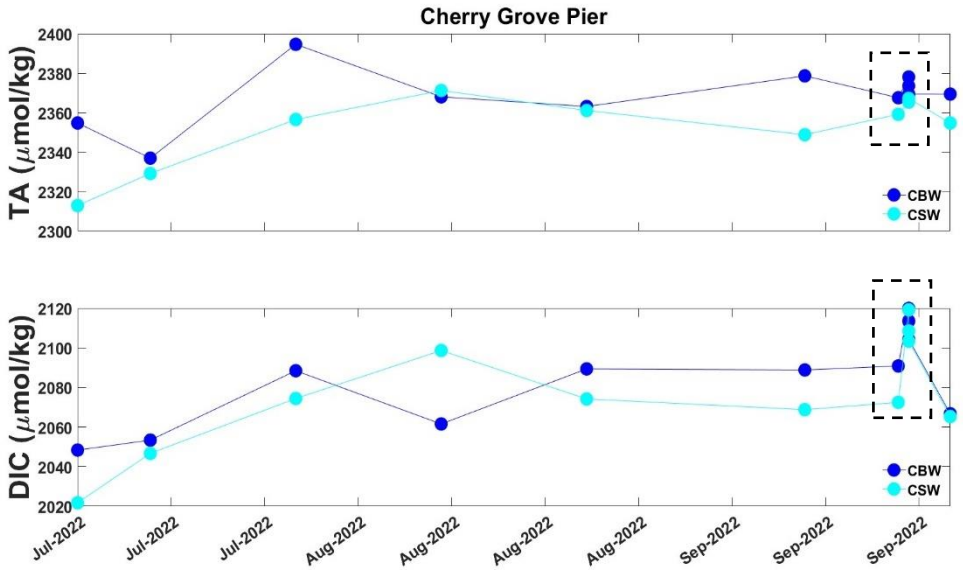

Figure 16. TA (μmol/kg) and DIC (μmol/kg) at Cherry Grove Pier from July 2022 to September 2022 due to Hurricane Ian damage at the pier. Error bars are smaller than the marker. Cherry Grove bottom water (CBW) = blue and Cherry Grove surface water (CSW) = cyan. Black dashed boxes represent diurnal sampling zoomed in for Figure 19.

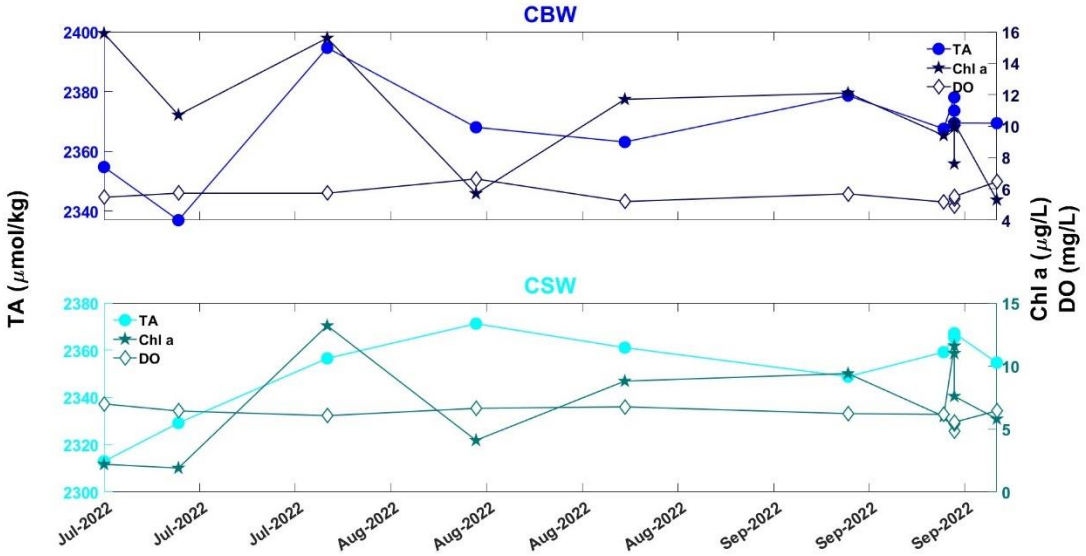

Figure 17. TA, Chl a and DO at Cherry Grove Pier (CBW and CSW) from the sampling period (July 2022 to September 2022). TA = circles, Chl a = stars, DO = open diamonds. Diurnal sampling took place from September 22, 2022 at 22:30 to September 23, 2022 at 10:30.

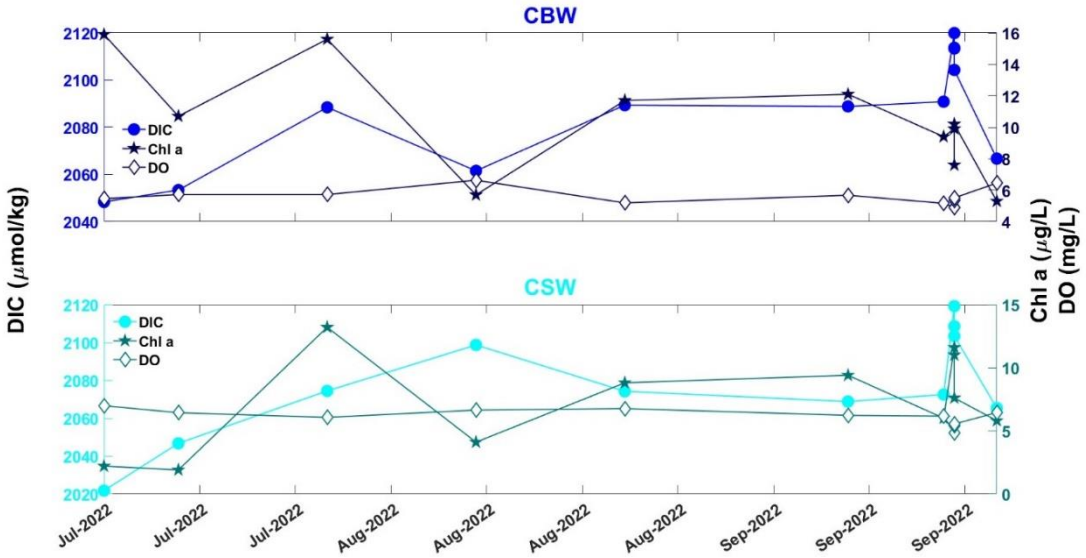

Figure 18. DIC, Chl a and DO at Cherry Grove Pier (CBW and CSW) from the sampling period (July 2022 to September 2022). DIC = circles, Chl a = stars, DO = open diamonds.

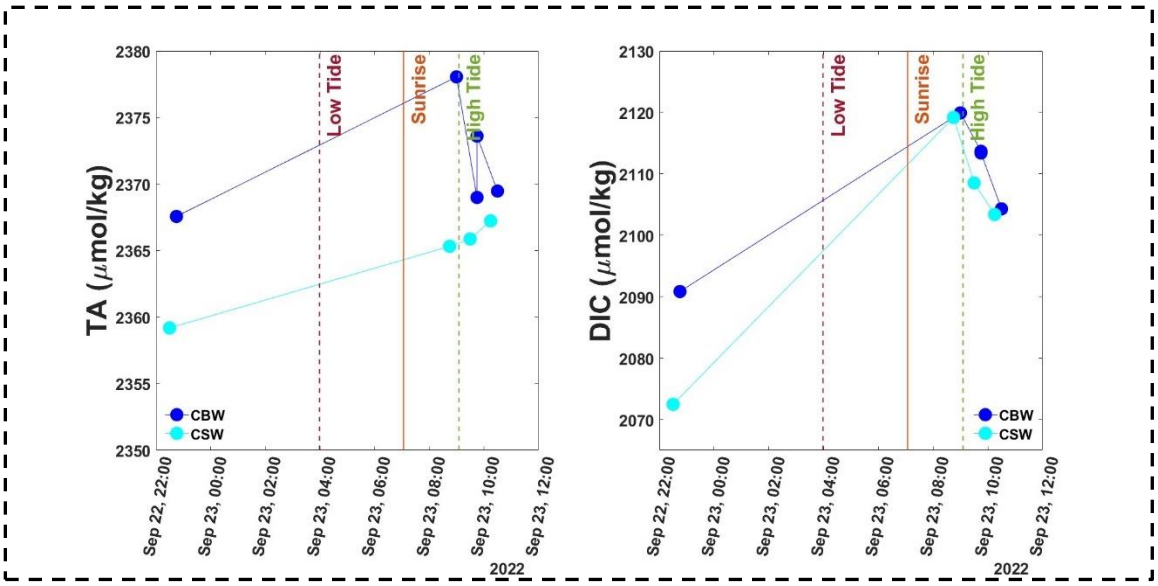

Figure 19. Diurnal pre-Hurricane Ian sampling for TA (μmol/kg) and DIC (μmol/kg) at Cherry Grove Pier. Sampling took place from September 22, 2022 at 22:30 to September 23, 2022 at 10:30. Lines represent low tide (dark red dashed line) at 03:59, high tide (green dashed line) at 09:05 and sunrise (orange solid line) at 07:04.

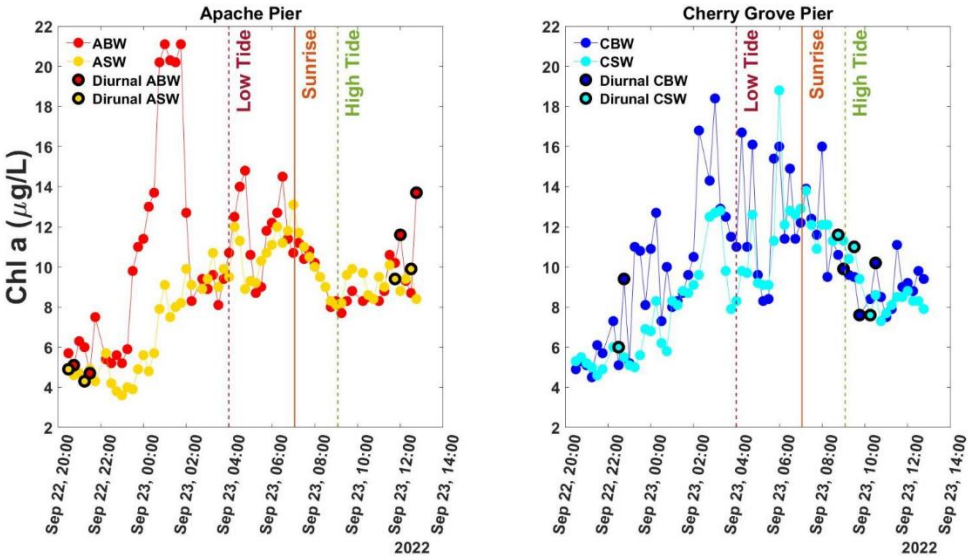

Figure 20. Chl a (µg/L) sensor values from Apache and Cherry Grove Pier corresponding with diurnal sampling that took place in Figure 15 and Figure 19. Sampling took place from September 22, 2022 at 22:30 to September 23, 2022 at 10:30. Lines represent low tide (dark red dashed line) at 03:59, high tide (green dashed line) at 09:05 and sunrise (orange solid line) at 07:04. Black outlined points correspond with discrete DIC and TA samples from Figure 15, Figure 19.

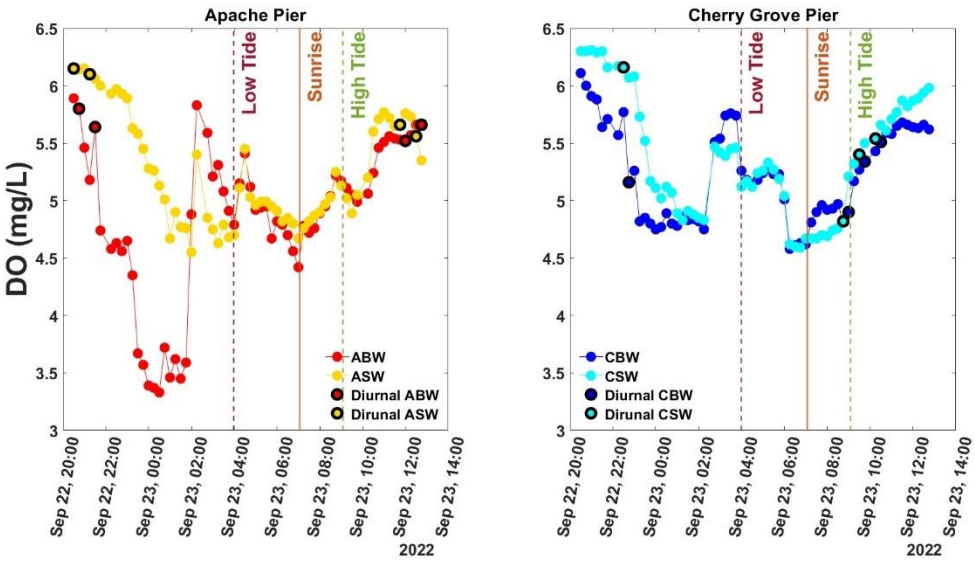

Figure 21. DO (mg/L) sensor values from Apache and Cherry Grove Pier corresponding with diurnal sampling that took place in Figure 15 and Figure 19. Sampling took place from September 22, 2022 at 22:30 to September 23, 2022 at 10:30. Lines represent low tide (dark red dashed line) at 03:59, high tide (green dashed line) at 09:05 and sunrise (orange solid line) at 07:04. Black outlined points correspond with discrete DIC and TA samples from Figure 15, Figure 19.

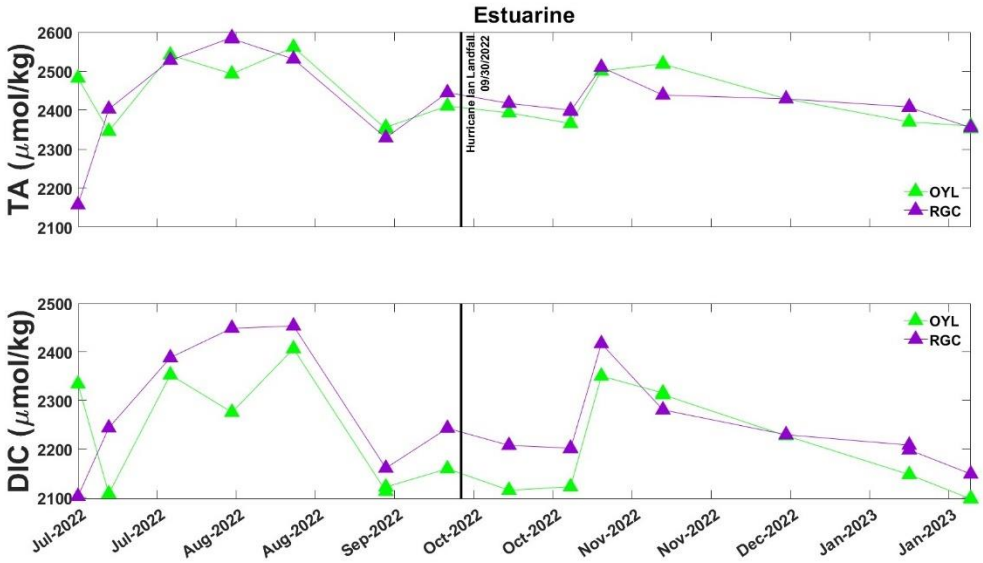

Figure 22. TA (μmol/kg) and DIC (μmol/kg) for the estuary sites from July 2022 to February 2023. Black vertical bars represent when Hurricane Ian made landfall on 9/30/2022. Error bars are smaller than the marker. Oyster Landing (OYL) = green and Rum Gully Creek (RGC) = purple.

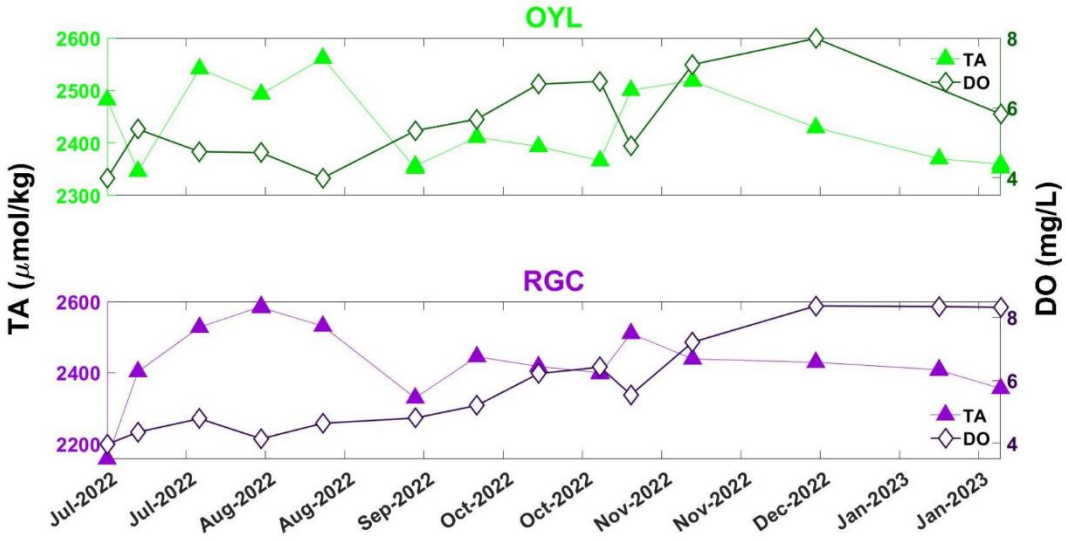

Figure 23. TA and DO at the estuarine sites (OYL and RGC) from the full COA sampling period (July 2022 to February 2023). TA = triangles, DO = open diamonds.

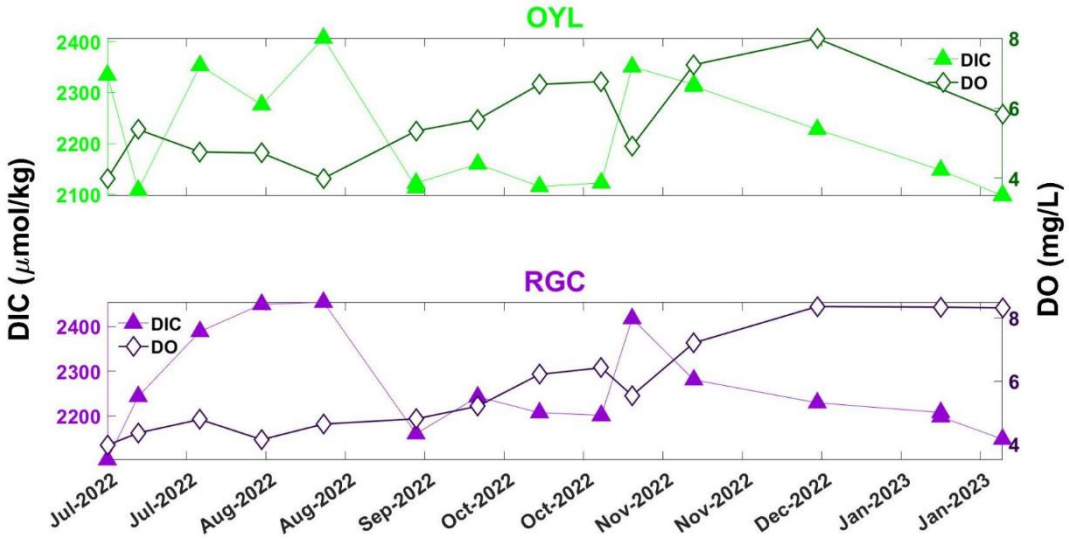

Figure 24. DIC and DO at the estuarine sites (OYL and RGC) from the full COA sampling period (July 2022 to February 2023). DIC = triangles, DO = open diamonds.

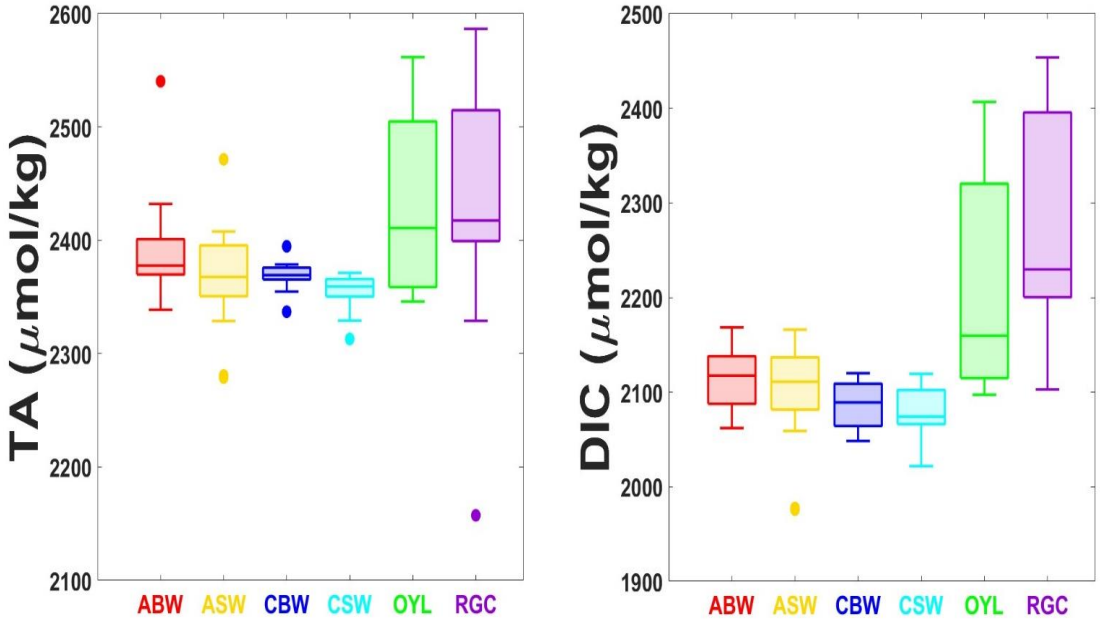

Figure 25. Box plots of TA and DIC from July 2022 to February 2023. Different colors represent site locations (ABW = red, ASW = yellow, CBW = blue, CSW = cyan, OYL = green, RGC = purple). Dots represent outliers which are data points more than 1.5 times the interquartile range away from the bottom or top of the box.

nTA vs. nDIC

Graphs of nTA versus nDIC at each site for the full sampling period are shown in Figure 26. The upper right quadrant of each graph denotes net community respiration and net community carbonate dissolution as well as TA and DIC values greater than the mean values from the sampling period (Figure 26) (Hall et al. 2024). The lower left quadrant shows the net community production (NCP) and net community calcification (NCC) (Figure 26) (Hall et al. 2024). The estuarine sites both have very strong linear relationships signifying that NCP and NCC have a strong influence on the carbonate system at these sites (Figure 26) (Hall et al. 2024). All six stations had more occurrences of photosynthesis and calcification (PC), data points in the lower left quadrant, than respiration and dissolution (RD), photosynthesis and dissolution (PD) and respiration and calcification (RC) for the full sampling period (Table 5). At ABW, ASW, CBW and CSW the number of outliers was greater than the number of PC occurrences (Table 5).

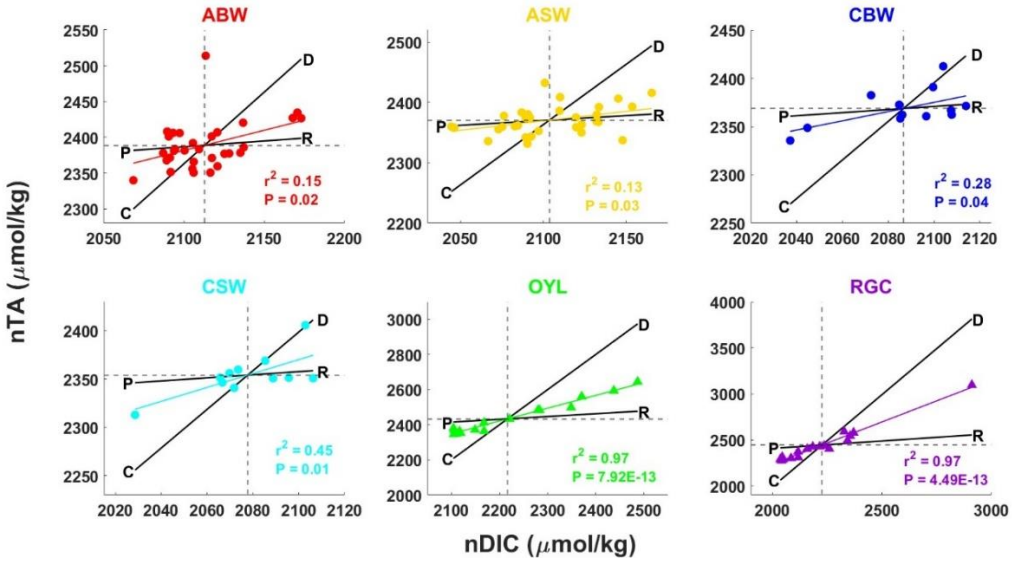

Figure 26. nTA vs. nDIC from July 2022 to February 2023. Points in the upper right quadrant indicate carbonate dissolution (D) and respiration (R) were dominant. Points in the lower left quadrant indicate photosynthesis (P) and calcification (C) were dominant (Hall et al. 2024). Dashed lined represent the mean nDIC and nTA at each station. Colored lines indicate linear regressions for all stations.

Table 5. Number of occurrences during dominance of photosynthesis and calcification (PC, lower left quadrat), respiration and dissolution (RD, upper right quadrat), photosynthesis and dissolution (PD, upper left quadrat), and respiration and calcification (RC, lower right quadrat) and the total sample sizes (n) throughout the full sampling period at each station. ±NCP is positive or negative net community production and ±NCC is positive or negative net community calcification.

Station	**PC dominance (+NCP, +NCC)**	**RD dominance (-NCP, -NCC)**	**PD dominance (+NCP, -NCC)**	**RC dominance (-NCP, +NCC)**	**Total Samples (n)**
ABW	12	7	5	7	31
ASW	11	8	7	6	32
CBW	4	3	2	3	12
CSW	4	2	2	3	11
OYL	10	6	0	1	17
RGC	10	5	0	2	17

Carbonate System Calculations

A Kruskal-Wallis test showed that there is very strong evidence ($P < 0.01$) that there is a difference between all six sites for each carbonate system parameter (Table 6). Calculated carbonate system concentrations at ABW, ASW, CBW, CSW, OYL and RGC show directly related patterns between TA, DIC, pH_T and Ω_{AR} (Figure 27, Figure 28, Figure 29). In the warmer summer months when water temperature is higher (Figure 5, Figure 6, Figure 7), pCO_2 (µatm) increased (Figure 27, Figure 28, Figure 29). When pCO_2 and H^+ (nmol/kg) increase, pH_T and Ω_{AR} decrease (Figure 27, Figure 28, Figure 29, Figure 30, Figure 31). There are increased pH_T and Ω_{AR} values at ABW and ASW on November 28th, 2022 with corresponding decreased pCO_2 and H^+ values. On November 1st, 2022 at ASW there are increased pCO_2 and H^+ values with corresponding decreased pH_T and Ω_{AR} values. Estuarine sites have the largest range for pCO_2 and pH_T (Figure 30).

Eastern Oysters (*Crassostrea virginica)* at their early life-stages that were exposed to pCO_2 values greater than 750, pH_T values less than 7.93, Ω_{CA} less than 2.82 ± 0.06 and Ω_{AR} less than 1.83 ± 0.04, were found to be smaller, slower to metamorphose and less calcified as well as having thinner shells resulting in being more vulnerable to predation (Gobler and Talmage 2014). Chambers et al. 2014 found that Summer Flounder (*Paralichthys dentatus*) embryo survival decreased by 48% when exposed to pCO_2 above 775 and pH_T below 7.8 (Figure 30) (Chambers et al. 2014). The estuarine sites fall above and below the thresholds that were found to be detrimental to the Eastern Oysters and the Summer Flounder (Figure 30, Figure 31).

The global area-averaged Ω_{CA} from 2015 is 4.54. This value has decreased by 0.12 per decade since 1975 (Feely et al. 2023). All six stations fall below that threshold from our full sampling period (Figure 31). Röckstrom et al. 2009 proposed a boundary for Ω_{AR} for global surface water at 2.75. ABW, ASW, OYL and RGC all fall below that boundary (Figure 31).

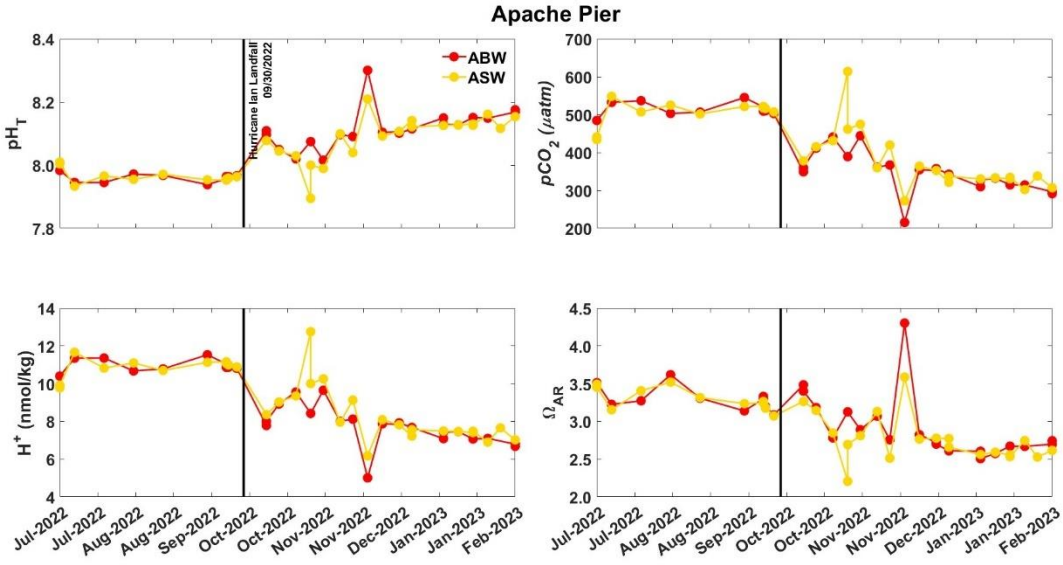

Figure 27. Carbonate System parameters for Apache Pier from July 2022 to February 2023. Black vertical bars represent when Hurricane Ian made landfall on 9/30/2022.

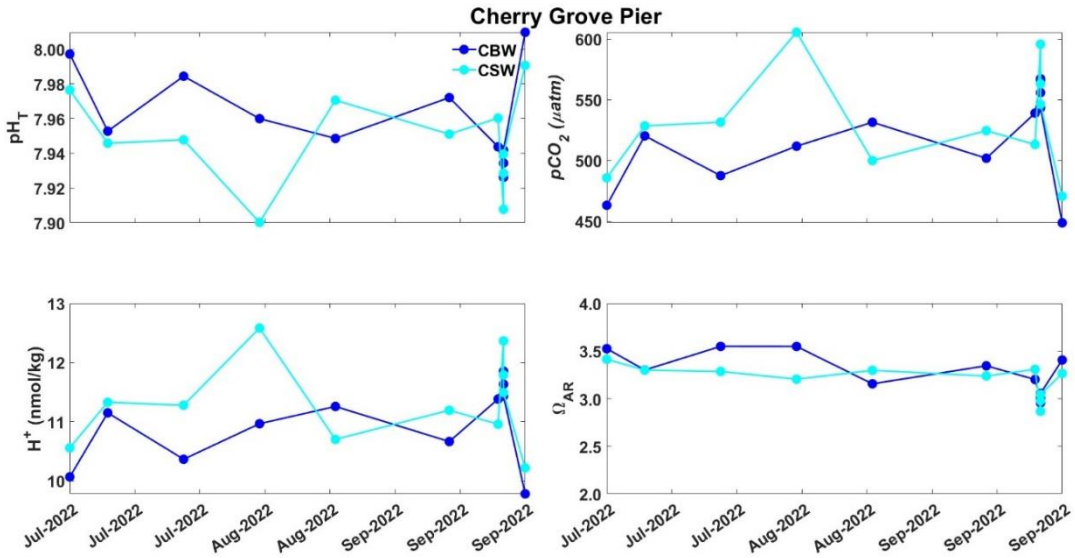

Figure 28. Carbonate System parameters for Cherry Grove Pier from July 2022 to September 2022 due to Hurricane Ian damage to the pier.

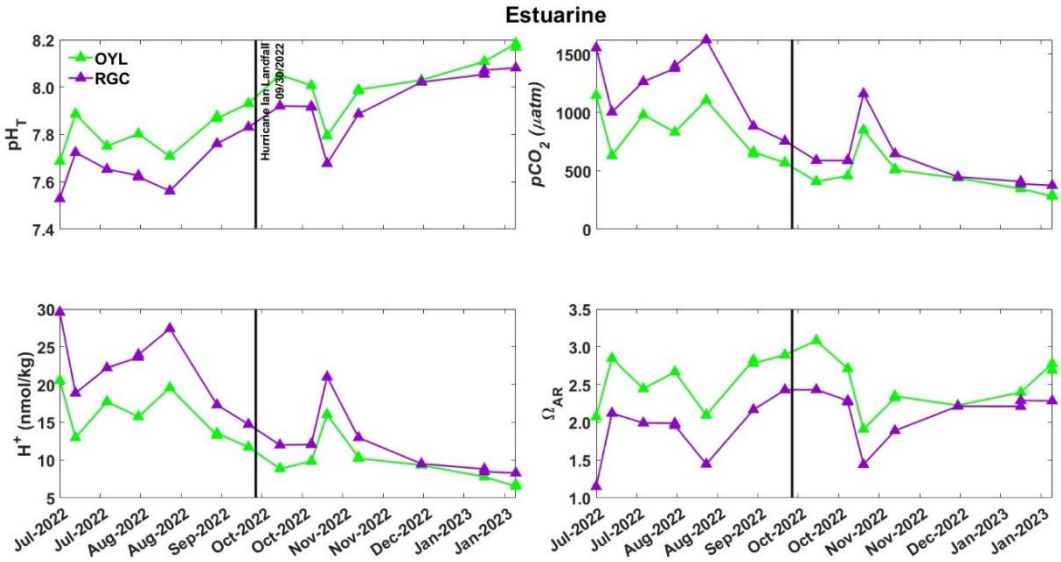

Figure 29. Carbonate System parameters for the estuary sites from July 2022 to February 2023. Black vertical bars represent when Hurricane Ian made landfall on 9/30/2022.

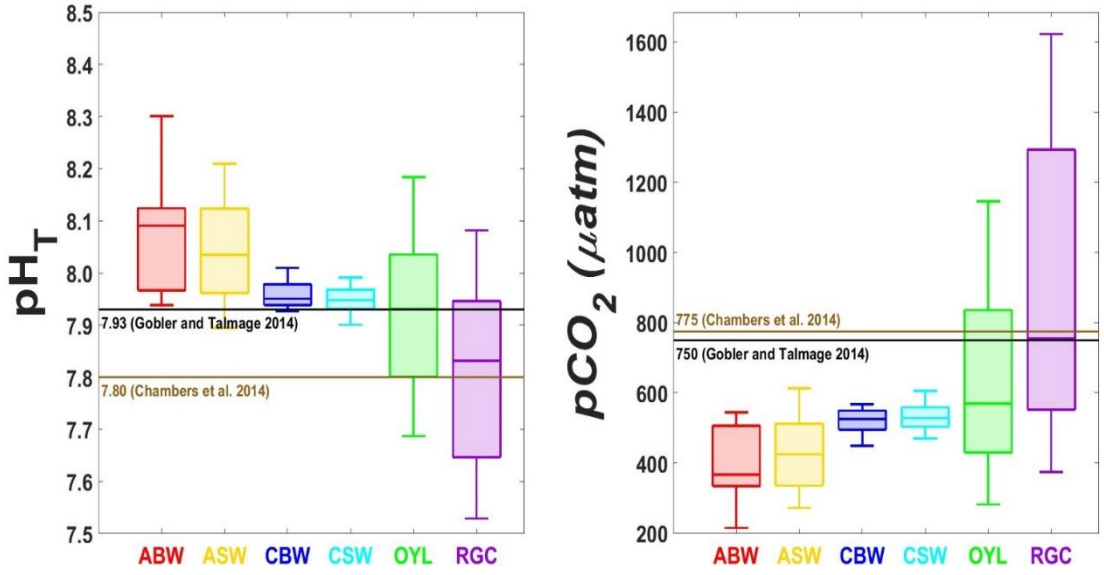

Figure 30. Box plots of pH_T calculated from CO2SYS and pCO_2 from July 2022 to February 2023. Different colors represent site locations (ABW = red, ASW = yellow, CBW = blue, CSW = cyan, OYL = green, RGC = purple). Dots represent outliers in the data. Thresholds for local organisms are represented by the solid horizontal lines: Summer Flounder (Chambers et al. 2014) = brown, Eastern Oysters (Gobler and Talmage 2014) = black.

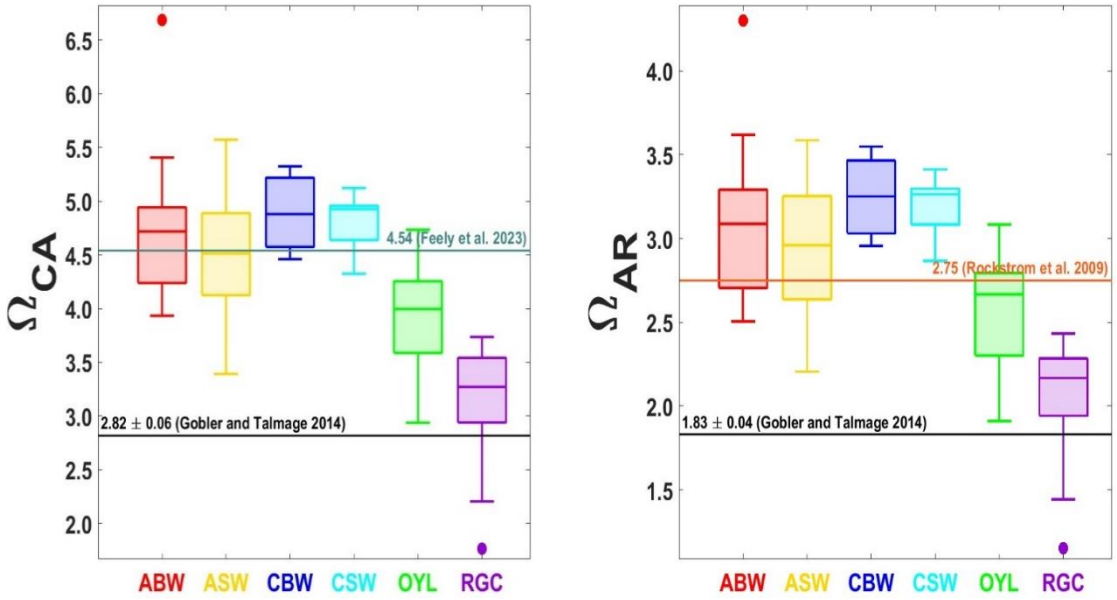

Figure 31. Box plots of Ω_{CA} and Ω_{AR} from July 2022 to February 2023. Different colors represent site locations (ABW = red, ASW = yellow, CBW = blue, CSW = cyan, OYL = green, RGC = purple). Dots represent outliers which are data points more than 1.5 times the interquartile range away from the bottom or top of the box. Thresholds are represented by the colored lines and values: Global area-averaged calcite saturation from 2015 (Feely et al. 2023) = teal, Proposed boundary for global surface water aragonite saturation (Rockström et al. 2009) = orange and Eastern Oysters (Gobler and Talmage 2014) = black.

Table 6. Results of Kruskal-Wallis test for computed carbonate system parameter concentrations between all six sites. Results indicate very strong evidence ($P < 0.01$) of a difference between all six sites for each carbonate system parameter.

Parameter	**P-value**	**df**
pH_T	P = 1.39E-07	5
pCO_2	P = 7.43E-08	
H^+	P = 1.39E-07	
Ω_{AR}	P = 5.91E-12	

pH_{NBS} vs. pH_T

Sensor pH_{NBS} measurements were directly compared to calculated pH_T measurements (Figure 32, Figure 34). The estuarine sites have the best fits at OYL and RGC with the highest r^2 values and highly significant P values (Figure 32, Table 7). The residuals for the estuarine sites are symmetric in distribution indicating a small difference between the measured pH_T and the modeled pH_T (Figure 33). The coastal-ocean pier sites have the lowest r^2 values at ABW, ASW, CBW and CSW (Figure 32, Table 7) and the residuals are left or right skewed for all (Figure 33). The majority of the calculated pH_T values fall within the sensor's post calibration check acceptance ranges for pH_{NBS} all sites (Figure 34).

Diurnal sampling at the coastal-ocean stations show that at Apache Pier, pH_T increases between samples at both ABW and ASW on September 22 in the evening and at ABW in the morning on September 23. ASW on September 23 in the morning doesn't change between samples (Figure 35). At Cherry Grove Pier CSW is higher than CBW on September 22 in the evening. CBW and CSW decrease overnight to then increase after high tide on September 23 in the morning (Figure 35).

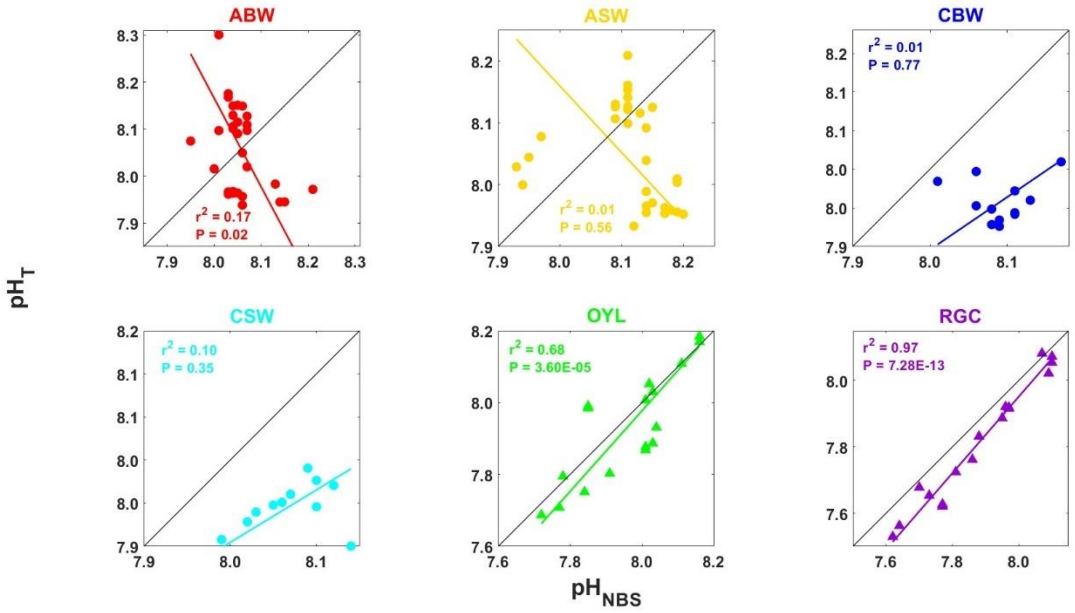

Figure 32. pH_T vs. pH_{NBS} sampled from July 2022 to February 2023. Black line represents 1:1 line. See statistics in Table 7.

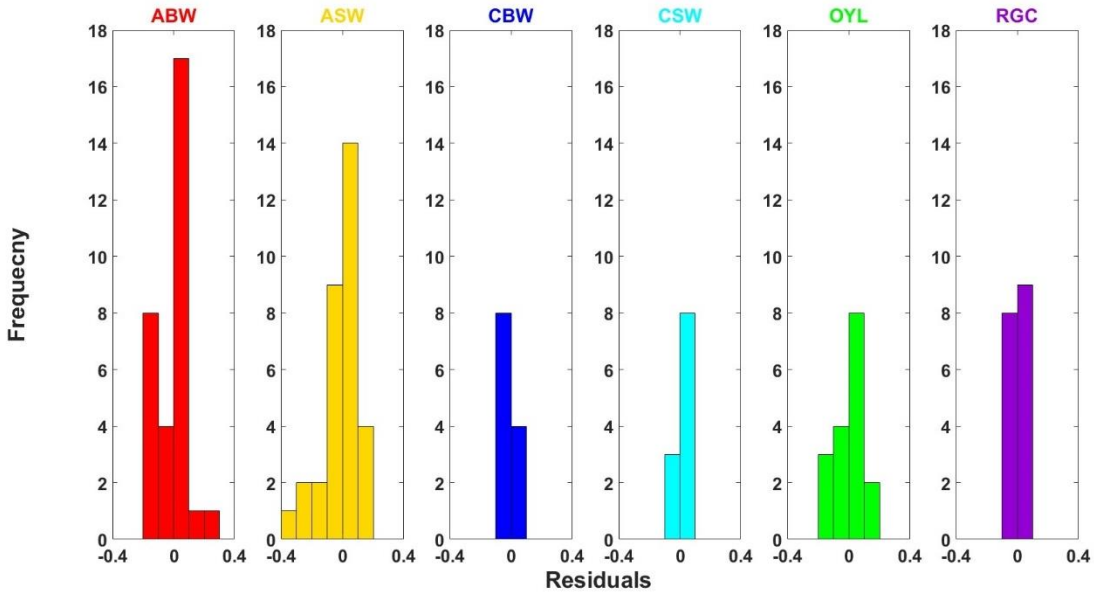

Figure 33. Residuals for pH_T vs. pH_{NBS}. Bins are 0.1.

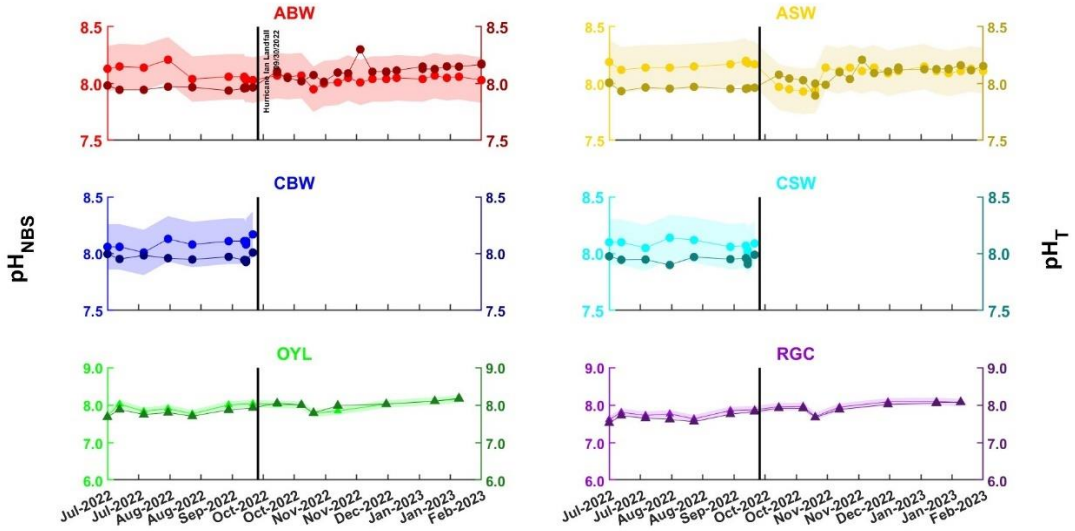

Figure 34. pH_{NBS} and pH_T sampled from July 2022 to February 2023 with shaded areas representing the instrument's post calibration check acceptance range (±0.2 for ABW, ASW, CBW, CSW and ±0.1 for OYL, RGC (see Table 2 for more details)). The vertical black line represents when Hurricane Ian made landfall in South Carolina on 09/30/2022. pH_{NBS} = Light colored symbols and lines and pH_T = Dark colored symbols and lines.

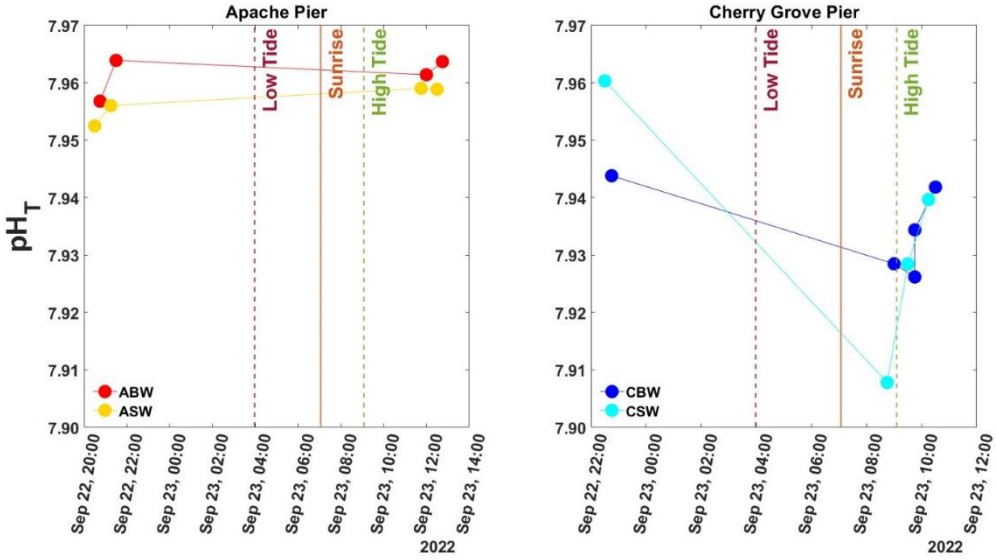

Figure 35. pH_T calculated from sampling during September 22, 2022 20:30 to September 23, 2024 12:45 at the coastal-ocean pier sites (Apache Pier and Cherry Grove Pier). Dashed lines represent times of tides and sunrise (Low tide = dark red, high tide = green, sunrise = orange).

Total Alkalinity (μmol/kg) vs. Salinity (ppt)

The coastal-ocean pier surface water sites have the highest r^2 values at ASW and CSW (Figure 36, Table 7). P values are highly significant at ABW, ASW, CSW and RGC (Figure 36, Table 7). The coastal-ocean pier bottom water and estuarine sites show much weaker r^2 values including ABW, CBW, OYL and RGC (Figure 36, Table 7). The residuals for the coastal-ocean pier sites (ABW, ASW, CBW, CSW) are symmetric in distribution indicating a small difference between the measured TA and the modeled TA (Figure 37).

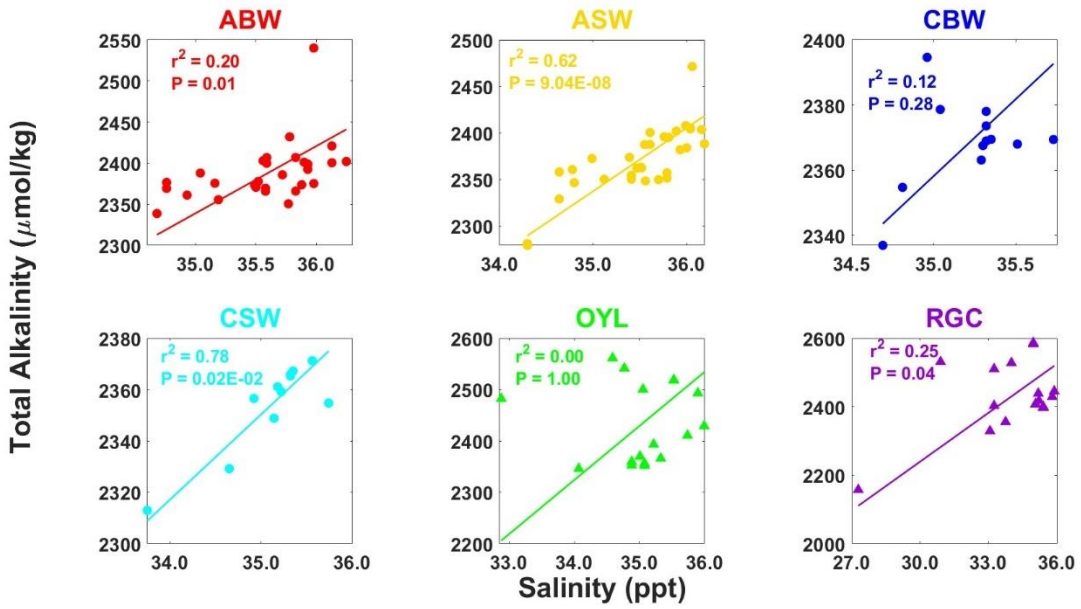

Figure 36. Total Alkalinity (μmol/kg) vs. Salinity (ppt) sampled from July 2022 from February 2023.

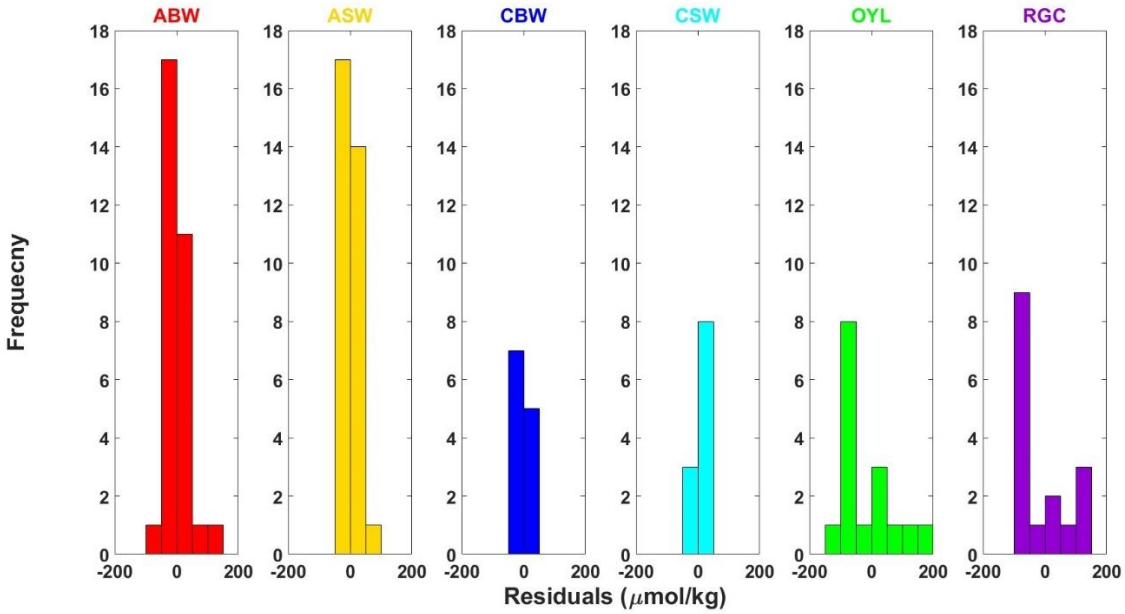

Figure 37. Residuals for Total Alkalinity (μmol/kg) vs. Salinity (ppt). Bins are 50.

Table 7. Results of the Regression analysis for linear relationships between parameters using Geometric Mean Regression (GMR) including the coefficient of determination (r^2), p-value (P) and sample size (n). The slope (m) and y-intercept (b) describe the line of best fit.

Station	**pH_T vs. pH_{NBS}**	**TA vs. Salinity**
ABW	P = 0.02* r^2 = 0.17 n = 31 m = -1.887 b = 23.26	P = 0.01* r^2 = 0.20 n = 31 m = 81.69 b = -520.1
ASW	P = 0.56 r^2 = 0.01 n = 32 m = -1.077 b = 16.78	P = 9.04E-08* r^2 = 0.62 n = 32 m = 68.24 b = -51.22
CBW	P = 0.77 r^2 = 0.01 n = 12 m = 0.6805 b = 2.452	P = 0.28 r^2 = 0.12 n = 12 m = 47.20 b = 706.1
CSW	P = 0.35 r^2 = 0.10 n = 11 m = 0.6092 b = 3.031	P = 0.02E-02* r^2 = 0.78 n = 11 m = 33.19 b = 1189
OYL	P = 3.60E-05* r^2 = 0.68 n = 17 m = 1.122 b = -1.000	P = 1.00 r^2 = 0.00 n = 17 m = 105.2 b = -1252
RGC	P = 7.28E-13* r^2 = 0.97 n = 17 m = 1.152 b = -1.268	P = 0.04* r^2 = 0.25 n = 17 m = 47.53 b = 813.6

*p-value less than 0.05

Covariance of pH_T with Other Water Quality Parameters

Statistically significant covariance of pH_T with salinity (ppt), temperature (°C) and DO (mg/L) was observed at most stations (Figure 38, Figure 39 and Figure 40, Table 8). Salinity has a statistically significant relationship with pH_T at RGC. This relationship is weaker at all other stations (Figure 38, Table 8). Temperature has a statistically significant negative correlation with pH_T at ABW, ASW, OYL and RGC. This relationship is weaker at CBW and CSW (Figure 39, Table 8). pH_T and DO have a statistically significant positive correlation at ABW, ASW, CBW, OYL and RGC. DO has a weaker relationship with pH_T at CSW (Figure 40, Table 8).

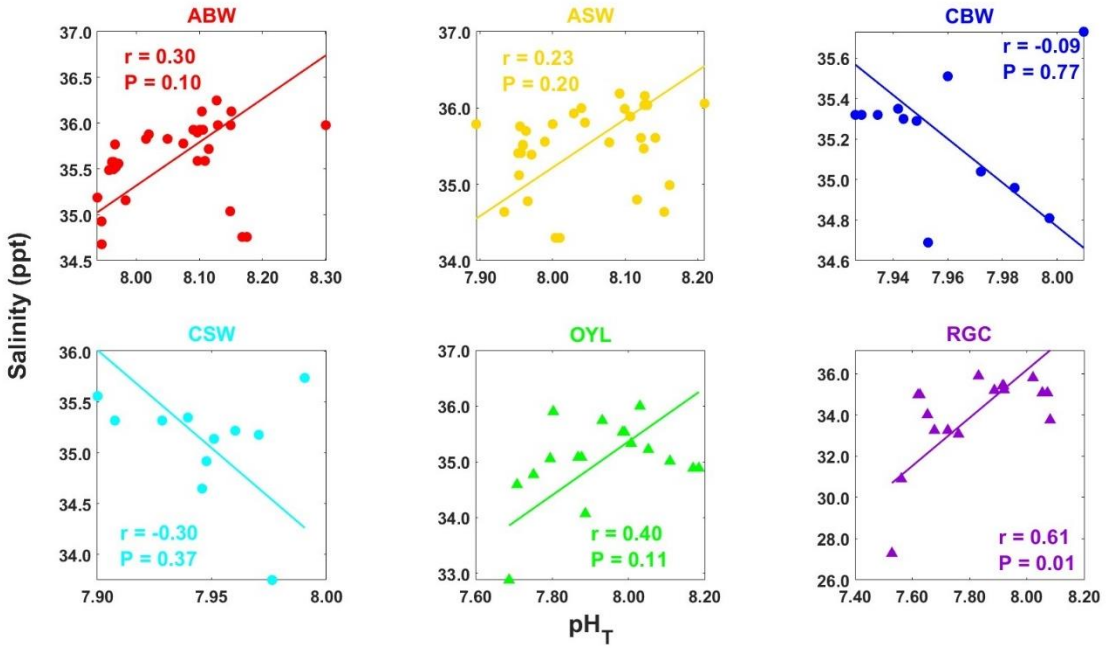

Figure 38. Salinity (ppt) vs. pH_T sampled from July 2022 to February 2023.

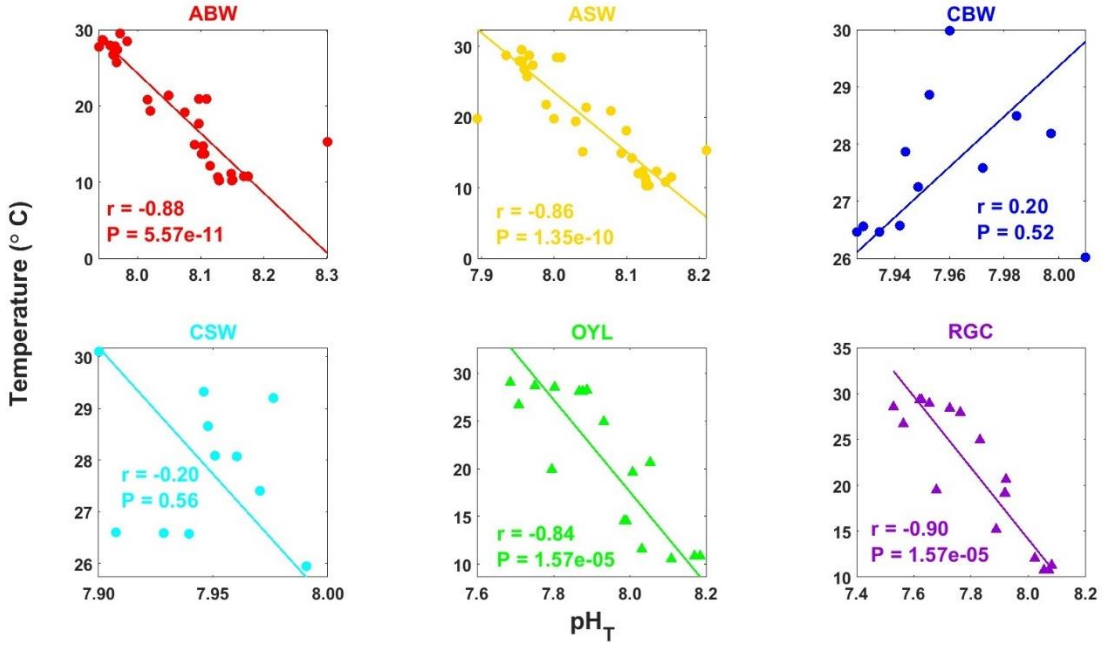

Figure 39. Temperature (°C) vs. pH_T sampled from July 2022 to February 2023.

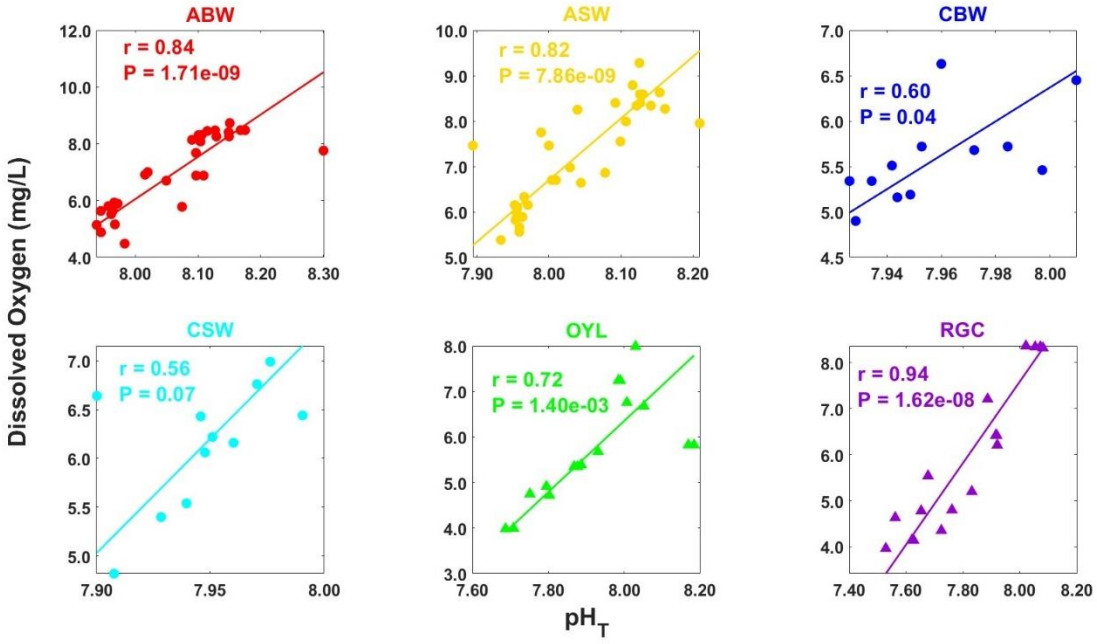

Figure 40. Dissolved Oxygen (mg/L) vs. pH_T sampled from July 2022 to February 2023.

*Table 8. Results of Regression analysis for linear relationships between pH_T and salinity (ppt), temperature (°C) and dissolved oxygen (mg/L) using Geometric Mean Regression (GMR) including the correlation coefficient (r), p-value (P) and sample size (n). The slope (m) and y-intercept (b) denote the line of best fit. *p-value < 0.05.*

Station	**Salinity (ppt) vs. pH_T**	**Temperature (°C) vs. pH_T**	**DO (mg/L) vs. pH_T**
ABW	P = 0.10 r = 0.30 n = 31 m = 4.729 b = -2.508	P = 5.57E-11* r = -0.88 n = 31 m = -78.41 b = 651.5	P = 1.71E-09* r = 0.84 n = 31 m = 14.88 b = -113.0
ASW	P = 0.20 r = 0.23 n = 32 m = 6.348 b = -15.56	P = 1.35E-10* r = -0.86 n = 32 m = -84.20 b = 697.1	P = 7.86E-09* r = 0.82 n = 32 m = 13.62 b = -102.2
CBW	P = 0.77 r = -0.09 n = 12 m = -10.81 b = 121.3	P = 0.52 r = 0.20 n = 12 m = 44.08 b = -323.3	P = 0.04* r = 0.60 n = 12 m = 18.66 b = -142.9
CSW	P = 0.37 r = -0.30 n = 11 m = -19.34 b = 188.8	P = 0.56 r = -0.20 n = 11 m = -49.00 b = 417.3	P = 0.07 r = 0.56 n = 11 m = 23.42 b = -180.0
OYL	P = 0.11 r = 0.40 n = 17 m = 4.816 b = -3.168	P = 1.57E-05* r = -0.84 n = 17 m = -48.36 b = 404.5	P = 1.40E-03* r = 0.72 n = 16 m = 7.803 b = -56.07
RGC	P = 0.01* r = 0.61 r^2 = 0.38 n = 17 m = 11.64 b = -56.96	P = 7.14E-07* r = -0.90 r^2 = 0.80 n = 17 m = -38.97 b = 325.8	P = 1.62E-08* r = 0.94 r^2 = 0.88 n = 17 m = 8.863 b = -63.31

Discussion

In-situ observations

In-situ observations from the full sampling period show seasonal trends for some of the parameters. From the summer to the winter months, water temperature decreases and DO increases (Figure 5, 6 and 7) (Buzzelli et al. 2009, Sanger et al. 2012). Salinity is driven by more than just evaporation and precipitation in these systems with periodic spikes and drops throughout the sampling period (Figure 5, Figure 6, Figure 7). These parameters can to be influenced by potential groundwater inputs (Viso et al. 2010), terrestrial runoff (Dafner et al. 2007), wind driven ocean surface currents (Troup et al. 2017), offshore water masses (Sanger et al. 2012), and riverine inputs (Xia et al. 2007) moving through the system.

Samples were collected from July 2022 to February 2023 at ABW, ASW, OYL and RGC. CBW and CSW samples were only collected from July to September 2022. There is a bias of record due not having a fully seasonal cycle for ABW, ASW, OYL and RGC and the limited seasonal representation is even narrower for CBW and CSW. Comparing ranges of parameters from the COA sampling period to sensor readings from 2022-2023 (Figure 8, Figure 9, Figure 10, Figure 11) shows that at CBW and CSW we

did not capture a vast majority of the ranges that are normally observed with a longer sampling period (Figure 8, Figure 9, Figure 10, Figure 11).

Temperature has a much larger range from the sensor readings from 2022 – 2023 then compared to the COA sampling period at CBW and CSW (Figure 8) signifying that a large portion of the range was not captured during the COA sampling period. At ABW, ASW, OYL and RGC the temperature ranges from the 2022 – 2023 sensor readings compared to the COA sampling period are similar (Figure 8) indicating at these sites, temperature ranges were adequately captured.

The estuarine sites have similar ranges for DO and pH_{NBS} between the 2022-2023 all sensor readings and the COA sampling period when compared (Figure 9, Figure 11). However, DO and pH_{NBS} at the coastal-ocean pier sites have much wider ranges from the 2022-2023 all sensor readings then the COA sampling period (Figure 9, Figure 11). These wider ranges indicate that numerous low pH events were not captured during the COA sampling period. Low pH co-occurs with low DO (Figure 5, Figure 6, Figure 7, Figure 40) due to high respiration rates of nutrient enriched organic matter coupled with water column stratification (Wallace et al. 2014, Gobler and Baumann 2016, Hall et al. 2024). Previous work has shown that low DO events frequently co-occur with increasing stable vertical thermal stratification in Long Bay, SC. Decreasing wind speed and stable salinity stratification also co-occur with low DO events (Sanger et al. 2012, Troup et al. 2017). Not capturing the full range of pH_{NBS} and DO at ABW, ASW, CBW and CSW may have resulted in missing low pH and low DO events that often co-occur.

Sample analysis results

Diurnal Sampling

Diurnal sampling for DIC and TA shows that ABW is higher than ASW for both DIC and TA. DIC for ABW, ASW, CBW and CSW increases overnight from September 22 to September 23 (Figure 15, Figure 19). These increases are likely due to respiration taking place at night in both the surface and bottom waters (Melzner et al. 2013, Baumann et al. 2015) (Figure 20, Figure 21). DIC at ABW increases after sunrise due to an increase in chl a and the bottom water being light limited therefore respiration taking place (Figure 15, Figure 20, Figure 21) (Redfield et al. 1963, Feely et al. 2018). DIC decreases alongside an increase in chl a at ASW after sunrise due to photosynthesis (Figure 15, Figure 20, Figure 21). At night, ASW is respiration dominant due to being light limited and therefore an increase in DIC (Figure 15, Figure 21). DIC and chl a at CBW and CSW decrease in the morning after sunrise and after high tide. Incoming tides raise pH and DO levels in a system due to the lower biological productivity on the open ocean (Baumann et al. 2015) (Figure 19, Figure 21, Figure 35). Values are similar for DIC, temperature, DO and salinity at CBW and CSW denoting potential physical mixing taking place with high tide during this sampling (Figure 6, Figure 19, Figure 21) (Sanger et al. 2012, Troup et al. 2017).

TA and DIC

TA ranges from 2157 – 2587 and DIC ranges from 2097 - 2454 at OYL and RGC (Figure 22, Figure 25). TA at ABW, ASW, CBW and CSW ranges from 2279 – 2540 and

DIC ranges from 1978 – 2168 (Figure 12, Figure 16, Figure 25). The estuarine sites have larger ranges and values for DIC and TA than the coastal-ocean sites (Figure 25). Generally, higher salinity waters have higher alkalinity (Pimenta and Grear 2018) but the estuarine sites have slightly lower salinities with higher TA than the coastal-ocean pier sites (Figure 25) most likely from dissolved organic matter (DOM) (Cai et al. 1998, Yang et al. 2015) which acts as a proton acceptor, influencing the acid-base system of seawater (Kulinski et al. 2014, Kortazar et al. 2019). In areas with high DOM concentrations, organic alkalinity (TA-org) may be an important component of TA, in which case TA-org can greatly affect the calculations of the carbonate system using CO2SYS (Kulinski et al. 2014, Ko et al. 2016). Areas with high DOM have significant primary production and/or substantial inputs of DOM from terrestrial sources (Kulinski et al. 2014). Contributions of phytoplankton produced organic acids to TA of seawater can be substantial in productive coastal areas (Ko et al. 2016). Extreme highs and lows seen in TA and DIC (Figure 12, 13, 14, 16, 17, 18, 22, 23 and 24) are indications of system inputs and removal of TA and DIC from potential biogeochemical processes (i.e. respiration and photosynthesis) (Figure 13, 14, 17, 18, 23, 24). (Redfield et al. 1963, Suzuki and Kawahata 2003, Ko et al. 2016). Chl a increases and DO decreases associated with DIC increases indicates respiration taking place and adding CO_2 into the system (Figure 14, Figure 18, Figure 24) (Schulz and Riebesell 2013). TA peaks that coincide with chl a peaks and DO decreases are indicative of respiration as well (Figure 13, Figure 17, Figure 23).

nTA:nDIC

At the estuarine sites, strong linearity between nTA and nDIC indicates a strong influence of NCC and NCP on the carbonate system (Figure 26) (Hall et al. 2024). The estuarine sites had more PC dominant occurrences than RD dominant ones with very little outliers denoting that these sites are strongly influenced by NCC and NCP (Figure 26, Table 5). On the contrary, the coastal-ocean pier sites showed weak linearity between nTA and nDIC and broader distribution, with more PC than RD, PD and RC dominant occurrences (Figure 26, Table 5). Previous work on coral reefs has found it uncommon to observe data points in the upper left (PD) and lower right (RC) quadrants suggesting that these combinations of biogeochemical processes, photosynthesis-dissolution and respiration-calcification, may be rare on coral reefs (Muehllehner et al. 2016). The fairly even distribution of PC, RD, PD and RC dominant occurrences throughout the sampling period at coastal-ocean pier sites indicates that all these combinations of biogeochemical processes are taking place at some point (Figure 26, Table 5) and that these occurrences may be more common in these coastal-ocean environments.

Carbonate system calculations

pH_T, pCO_2, H^+, Ω_{CA} and Ω_{AR} were all calculated from DIC and TA values using CO2SYS. Murrells Inlet, commonly known as the seafood capital of South Carolina, is home to many local species including Eastern Oysters (*Crassostrea virginica).* Gobler and Talmage 2014 found that eastern oysters exposed to carbonate system parameter thresholds shown in Figure 30 and Figure 31, at their early life stages, were found to be smaller, slower to metamorphose and less calcified as well as having thinner shells

resulting in being more vulnerable to predation. OYL and RGC both had values that fell within the pH_T, pCO_2, Ω_{CA} and Ω_{AR} thresholds (Gobler and Talmage 2014) indicating periodic events where eastern oysters could be experiencing acidification events detrimental to their development. As an estuarine species, Eastern Oysters face additional stressors in addition to acidification, such as increasing temperatures, hypoxia and lack of food which have been shown to decrease survival rates of larvae (Talmage and Gobler 2011, 2012, Gobler and Talmage 2014, Gobler et al. 2014). Acidification in estuaries may be partially contributing to the 'functional extinction' that has been observed in numerous oyster populations globally throughout the past century (Beck et al. 2011, Gobler and Talmage 2014).

Myrtle Beach, SC is known for its excellent fishing and has over 14 million visitors per year (Myrtle Beach Fishing 2024). One of the species most sought after in the area to fish includes the Summer Flounder (*Paralichthys dentatus*). Chambers et al. 2014 found that Summer Flounder exposed to carbonate chemistry parameter thresholds shown in Figure 30, showed embryo survival rates decreasing by ~48%. The estuarine sites fell within the noted thresholds indicating that Summer Flounder may be experiencing a decrease in embryo survival rates during periods of high pCO_2 and low pH. Summer Flounder also face additional stressors including temperature change and hypoxia that combined with elevated pCO_2 is concerning and further extremes may force populations to move to different habitats in the future (Schwieterman et al. 2019).

Feely et al. 2023 showed that the global area-averaged Ω_{CA} from 2015 is 4.54. This value has decreased by 0.12 per decade since 1975 and all six stations fall below

that average from the full sampling period (Figure 31). This indicates that all six of the stations fall below the threshold that has been decreasing globally over the past 50 years. Röckstrom et al. 2009 proposed a boundary for Ω_{AR} for global surface water at 2.75 resulting in detrimental effects on many marine organisms documented. This threshold is well above the geochemical threshold of $\Omega_{AR} = 1$. ABW, ASW, OYL and RGC all fall below that boundary (Figure 31) signifying that these stations are already experiencing events where Ω_{AR} is below the boundary where detrimental effects on marine organisms are seen (Röckstrom et al. 2009) supporting hypothesis 3 that estuarine sites are more prone to acidification than coastal-ocean sites.

pH_{NBS} vs. pH_T

Comparing pH_{NBS} measured vs. pH_T calculated for the estuarine sites shows strong linearity between the two parameters signifying that using current sampling methodologies and sensors at these sites allows for pH_{NBS} to be used as a proxy for pH_T supporting hypothesis 1 (Figure 32, Figure 34, Table 7). At all the coastal-ocean pier sites the modeled pH fits only represented 1-17% of the measured pH data (Figure 32, Table 7) showing weak linearity. These weak relationships may be a consequence of not being able to capture the full range of pH_{NBS} values, especially the lower ones, normally occurring throughout a sampling year (Figure 11). At the estuarine sites, pH_{NBS} ranges were captured similarly during the COA sampling period and looking at the sensor readings from 2022-2023 (Figure 11). Capturing of the full range of pH_{NBS} values may be one of the reasons that pH_{NBS} showed much stronger linearity at the estuarine sites than compared to the coastal-ocean sites (Figure 11).

The majority of the calculated pH_T values fall within the sensor's post calibration field check acceptance range (Figure 34). The *in-situ* deployed coastal-ocean station meters are deployed continuously and have a higher variability range for pH_{NBS} than the estuarine sites (Figure 34) exposing them to much more dynamic conditions.

Diurnal sampling at the coastal-ocean stations shows a decrease overnight in pH_T at CBW and CSW indicating respiration taking place over night due to light limitation (Figure 20, Figure 21, Figure 35) (Melzner et al. 2013, Baumann et al. 2015). pH_T at CBW and CSW increase after sunrise and high tide indicating photosynthesis (Figure 20, Figure 21, Figure 35). Incoming tides raise pH and DO levels in a system due to the lower biological productivity on the open ocean (Baumann et al. 2015) (Figure 21, Figure 35).

Total Alkalinity (µmol/kg) vs. Salinity (ppt)

TA and salinity exhibit a close linear relationship in the surface ocean because TA in the open ocean is mainly controlled by freshwater addition or removal, which is shown by changes in salinity (Millero et al. 1998, Jiang et al. 2014). However, TA can be altered by biogeochemical processes (i.e respiration and photosynthesis) (Jiang et al. 2014, Ko et al. 2016, Pimenta and Grear 2018) therefore, having higher variability in the coastal environments.

All six stations showed weak linearity between TA and salinity (Figure 36, Table 7). The coastal-ocean pier surface water sites (ASW and CSW) showed the strongest linear relationships out of all six stations with r^2 values of 0.62 and 0.78 (Figure 36, Table

7). This is due to the surface water mainly being affected by freshwater addition and removal through evaporation and precipitation (Millero et al. 1998, Jiang et al. 2014) and in the subtropical and tropical open ocean, variations in salinity account for more than 80% of the surface TA variability (Millero et al. 1998, Jiang et al. 2014). However, ASW and CSW do not exhibit strong enough relationships to indicate that TA can be calculated from salinity in the coastal zone. This indicates these sites have more complex and dynamic carbonate chemistry (Kerr et al. 2021) and that other processes may be affecting this relationship including biogeochemical processes especially respiration (Pimenta and Grear 2018), riverine inputs (Xia et al. 2007), terrestrial runoff (Dafner et al. 2007), upwelling groundwater (Viso et al. 2010), wind driven ocean surface currents (Troup et al. 2017) and offshore water masses (Sanger et al. 2012). TA-org which are organic molecules that contribute to TA, may also be having a large influence on TA calculations and the TA salinity relationship since coastal waters are greatly influenced by nutrient and carbon inputs that stimulate the production and remineralization of organic matter (Mallin et al. 2000, Sanger et al. 2012, Kerr et al. 2021).

Due to the lack of a conservative relationship between TA and salinity, calculating parameters (i.e pH_T, DIC, TA, pCO_2, Ω_{CA} and Ω_{AR}) for the historical data sets using this linear relationship was unable to be performed to evaluate hypothesis 2 which states that two coastal-ocean and two estuarine sites in Long Bay, SC have been experiencing decreasing pH and degree of saturation of calcite and aragonite over the past decade and that total alkalinity has a direct relationship with salinity (in addition to 1a).

Covariance of pH_T with other water quality parameters

pH_T was calculated from samples collected in conjunction with other water quality parameters at all six stations including temperature, salinity and DO. Statistical analyses at all sites for all parameters with pH_T suggest that multiple parameters are major contributors to pH_T variability (Table 8, Figure 38, 39 and 40). Temperature showed a strong negative correlation with pH_T at ABW, ASW, OYL and RGC (Figure 39, Table 8) signifying that pH_T decreases when temperature increase (Solomon et al. 2007) supporting hypothesis 4a stating pH has an inverse relationship with temperature. DO showed a strong positive correlation with pH_T at ABW, ASW, OYL and RGC (Figure 40, Table 8) denoting that pH_T decreases when DO decreases supporting hypothesis 4b stating pH has a direct relationship with DO. This is due to respiration taking place consuming O_2 and releasing CO_2 (Figure 14, Figure 20, Figure 21, Figure 24) (Redfield et al. 1963, Schulz and Riebesell 2013). CBW and CSW did not show significant correlation between pH_T vs. temperature or DO most likely due to the smaller sample size and narrower range of values captured (Figure 8, Figure 9).

Recommendations for future studies

Future studies should be done to obtain more observations and sampling to better identify potential acidification trends (Pimenta and Grear 2018). Identifying key biogeochemical processes that are altering the carbonate system is imperative. This should be done through the collection of nutrients (Wanninkhof et al. 2015, Cai et al. 2021, Kerr et al. 2021, Hall et al. 2024) and chl a data (Borges and Gypens 2010, Hall et al. 2024) at the estuarine sites. TA-org is most likely a major contributor to the non-conservative behavior of TA vs. salinity due to the highly organic blackwater riverine systems (Xia et al. 2007) and saltwater marshes that influence and move through these sites (Fassbender et al. 2017, Kerr et al. 2021). Due to the highly dynamic nature of these systems future sampling should also include measuring pH_T from discrete samples in the laboratory to compare CO2SYS calculated pH_T to the discretely measured pH_T to help identify areas of error (Dickson et al. 2007, Fassbender et al. 2017).

Obtaining a full seasonal dataset and the full range of parameter variability for pH and other parameters, would allow for better identification of seasonal variations at all the sites. Future projects would want to focus on collecting discrete samples throughout multiple large weather events (i.e. hurricanes) to determine if these events have been affecting acidification on both short- and long-term scales. To capture biogeochemical

processes (respiration and photosynthesis) and tidal influences, performing more diurnal samplings would allow for the identification of potential diurnal acidification variations (Baumann et al. 2015). There should also be a focus on identifying short term variability with respect to hypoxia and low pH events due to significant diurnal and seasonal variations with respect to the carbonate system (Melzner et al. 2013).

This study is also a call to try and find more cost-effective ways to study estuarine and coastal-ocean acidification trends. The dynamic nature of these systems makes them extremely difficult and expensive to study. Current methodologies include the collection of discrete water samples which are expensive to analyze. These systems have higher temporal and spatial variability of the carbonate system so the collection of higher frequency and spatially robust data to identify trends is needed (Keller et al. 2014, Pimenta and Grear 2018). All of these aspects make it difficult to study acidification trends in the coastal zone. There should be a future focus on the need for better and more holistic data collection (i.e. nutrients, carbonate parameters, water quality parameters, etc.) to better understand and describe potential acidification in these estuarine and coastal-ocean systems.

List of References

Bates, N.R., Y.M. Astor, M.J. Church, K. Currie, J.E. Dore, M. González-Dávila, L. Lorenzoni, F. Muller-Karger, J. Olafsson, and J.M. Santana-Casiano. 2014. A time-series view of changing ocean chemistry due to ocean uptake of anthropogenic CO2 and ocean acidification. Oceanography 27(1):126–141, http://dx.doi.org/10.5670/oceanog.2014.16.

Baumann, H., Wallace, R. B., Tagliaferri, T., & Gobler, C. J. (2015). Large natural pH, CO 2 and O 2 fluctuations in a temperate tidal salt marsh on diel, seasonal, and interannual time scales. Estuaries and Coasts, 38, 220-231.

Bauer, J. E., Cai, W. J., Raymond, P. A., Bianchi, T. S., Hopkinson, C. S., & Regnier, P. A. (2013). The changing carbon cycle of the coastal ocean. *Nature*, *504*(7478), 61-70. https://doi.org/10.1038/nature12857

Beck MW, Brumbaugh RD, Airoldi L, Carranza A, Coen LD, Crawford C, Defeo O, Edgar GJ, Hancock B, Kay MC, et al. (2011) Oyster reefs at risk and recommendations for conservation, restoration, and management. Bioscience 61: 107–116

Borges, A. V., & Gypens, N. (2010). Carbonate chemistry in the coastal zone responds more strongly to eutrophication than ocean acidification. Limnology and Oceanography, 55(1), 346-353.

Burnett, L. E. (1997). The challenges of living in hypoxic and hypercapnic aquatic environments. Am. Zool. 37, 633–640. doi: 10.1093/icb/37.6.633

Cai, W. J., Wang, Y., & Hodson, R. E. (1998). Acid-base properties of dissolved organic matter in the estuarine waters of Georgia, USA. Geochimica et Cosmochimica Acta, 62(3), 473-483.

Cai, W. J., Hu, X., Huang, W. J., Jiang, L. Q., Wang, Y., Peng, T. H., & Zhang, X. (2010). Alkalinity distribution in the western North Atlantic Ocean margins. Journal of Geophysical Research: Oceans, 115(C8).

Cai, W. J. (2011). Estuarine and coastal ocean carbon paradox: CO2 sinks or sites of terrestrial carbon incineration?. *Annual review of marine science*, *3*, 123-145. 10.1146/annurev-marine-120709-142723

Cai WJ, Feely RA, Testa JM, Li M, Evans W, Alin SR, Xu YY, Pelletier G, Ahmed A, Greeley DJ, Newton JA, Bednaršek N. Natural and Anthropogenic Drivers of Acidification in Large Estuaries. Ann Rev Mar Sci. 2021 Jan;13:23-55. doi: 10.1146/annurev-marine-010419-011004. Epub 2020 Sep 21. PMID: 32956015.

Carter, B. R., Williams, N. L., Evans, W., Fassbender, A. J., Barbero, L., Hauri, C., et al. (2019). Time of detection as a metric for prioritizing between climate observation quality, frequency, and duration. Geophysical Research Letters, 46, 3853–3861. https://doi.org/10.1029/2018GL080773

Chung, S. N., Park, G. H., Lee, K., Key, R. M., Millero, F. J., Feely, R. A., Sabine, C. L., & Falkowski, P. G. (2004). Postindustrial enhancement of aragonite undersaturation in the upper tropical and subtropical Atlantic Ocean: The role of fossil fuel CO2. Limnology and Oceanography, 49(2), 315-321. https://doi.org/10.4319/lo.2004.49.2.0315

Cochran, R. E., and Burnett, L. E. (1996). Respiratory responses of the salt marsh animals, Fundulus heteroclitus, Leiostomus xanthurus, and Palaemonetes pugio to environmental hypoxia and hypercapnia and to the organophosphate pesticide, azinphosmethyl. J. Exp. Mar. Biol. Ecol. 195, 125–144. doi: 10.1016/ 0022-0981(95)00102-6

Dafner, E. V., Mallin, M. A., Souza, J. J., Wells, H. A., & Parsons, D. C. (2007). Nitrogen and phosphorus species in the coastal and shelf waters of Southeastern North Carolina, Mid-Atlantic US coast. Marine Chemistry, 103(3-4), 289-303.

Dickson, A. G. (1990). Standard potential of the reaction: AgCl (s)+ 12H2 (g)= Ag (s)+ HCl (aq), and and the standard acidity constant of the ion HSO4− in synthetic sea water from 273.15 to 318.15 K. The Journal of Chemical Thermodynamics, 22(2), 113-127.

Dickson, A. G., Sabine, C. L., & Christian, J. R. (2007). *Guide to best practices for ocean CO2 measurements*. North Pacific Marine Science Organization. https://doi.org/10.25607/OBP-1342

Duarte, C.M., Hendriks, I.E., Moore, T.S. et al. Is Ocean Acidification an Open-Ocean Syndrome? Understanding Anthropogenic Impacts on Seawater pH. Estuaries and Coasts 36, 221–236 (2013). https://doi.org/10.1007/s12237-013-9594-3

Ekstrom, J. A., Suatoni, L., Cooley, S. R., Pendleton, L. H., Waldbusser, G. G., Cinner, J. E., et al. (2015). Vulnerability and adaptation of US shellfisheries to ocean acidification. Nat. Clim. Change 5, 207–214. doi: 10.1038/nclimate2508

Fassbender, A. J., Orr, J. C., and Dickson, A. G.: Technical note: Interpreting pH changes, Biogeosciences, 18, 1407–1415, https://doi.org/10.5194/bg-18-1407-2021, 2021.

Feely, R. A., Okazaki, R. R., Cai, W. J., Bednaršek, N., Alin, S. R., Byrne, R. H., & Fassbender, A. (2018). The combined effects of acidification and hypoxia on pH and aragonite saturation in the coastal waters of the California current ecosystem and the northern Gulf of Mexico. *Continental Shelf Research*, *152*, 50-60. https://doi.org/10.1016/j.csr.2017.11.002

Feely, R. A., Jiang, L. Q., Wanninkhof, R., Carter, B. R., Alin, S. R., Bednaršek, N., & Cosca, C. E. (2023). ACIDIFICATION OF THE GLOBAL SURFACE OCEAN. Oceanography, 36(2/3), 120-129.

Gattuso, J. P., Magnan, A., Billé, R., Cheung, W. W., Howes, E. L., Joos, F., Allemand, D., Bopp, L., Cooley, S. R., Eakin, C. M, Hoegh-Guldberg, O., Kelly, R. P., Pörtner, H. O., Rogers, A. D., Baxter, J. M., Laffoley, D., Osborn, D., Rankovic, A., Rochette, J., Sumaila, U. R., Treyer, S., & Turley, C. (2015). Contrasting futures for

ocean and society from different anthropogenic CO2 emissions scenarios. *Science*, *349*(6243), aac4722.

Gledhill, D.K., M.M. White, J. Salisbury, H. Thomas, I. Mlsna, M. Liebman, B. Mook, J. Grear, A.C. Candelmo, R.C. Chambers, C.J. Gobler, C.W. Hunt, A.L. King, N.N. Price, S.R. Signorini, E. Stancioff, C. Stymiest, R.A. Wahle, J.D. Waller, N.D. Rebuck, Z.A. Wang, T.L. Capson, J.R. Morrison, S.R. Cooley, and S.C. Doney. 2015. Ocean and coastal acidification off New England and Nova Scotia. Oceanography 28(2):182–197, https://doi.org/10.5670/oceanog.2015.41.

Gobler, C. J., & Talmage, S. C. (2014). Physiological response and resilience of early life-stage Eastern oysters (Crassostrea virginica) to past, present and future ocean acidification. Conservation Physiology, 2(1), cou004.

Gobler CJ, Depasquale EL, Griffith AW, Baumann H (2014) Hypoxia and acidification have additive and synergistic negative effects on the growth, survival, and metamorphosis of early life stage bivalves. PLoS One 9: e83648.

Gobler, C. J., & Baumann, H. (2016). Hypoxia and acidification in ocean ecosystems: coupled dynamics and effects on marine life. Biology letters, 12(5), 20150976.

Gran G. 1952. Determination of the equivalence point in potentiometric titrations. Part II. Analyst 77

Gruber, N., Clement, D., Carter, B. R., Feely, R. A., van Heuven, S., Hoppema, M., et al. (2019). The oceanic sink for anthropogenic CO2 from 1994 to 2007. Science 363, 1193–1199. doi: 10.1126/science.aau5153

Guinotte, J.M. and Fabry, V.J. (2008), Ocean Acidification and Its Potential Effects on Marine Ecosystems. Annals of the New York Academy of Sciences, 1134: 320-342. https://doi.org/10.1196/annals.1439.013

Hall ER, Wickes L, Burnett LE, Scott GI, Hernandez D, Yates KK, Barbero L, Reimer JJ, Baalousha M, Mintz J, Cai W-J, Craig JK, DeVoe MR, Fisher WS, Hathaway TK, Jewett EB, Johnson Z, Keener P, Mordecai RS, Noakes S, Phillips C, Sandifer PA, Schnetzer A and Styron J (2020) Acidification in the U.S. Southeast: Causes, Potential Consequences and the Role of the Southeast Ocean and Coastal Acidification Network. Front. Mar. Sci. 7:548. doi: 10.3389/fmars.2020.00548

Hall, E. R., Yates, K. K., Hubbard, K. A., Garrett, M. J., & Frankle, J. D. (2024). Nutrient and carbonate chemistry patterns associated with Karenia brevis blooms in three West Florida Shelf estuaries 2020-2023. Frontiers in Marine Science.

Hannides, A., Viso, D., Libes, S., Reimer, J., and Hall, E. (2021) Coastal and estuarine acidification in Long Bay, South Carolina. Grant proposal to South Carolina Sea Grant Consortium, 2022-24, pp 10

Hofmann GE, Smith JE, Johnson KS, Send U, Levin LA, et al. (2011) High-Frequency Dynamics of Ocean pH: A Multi-Ecosystem Comparison. PLOS ONE 6(12): e28983. https://doi.org/10.1371/journal.pone.0028983

Hu, X., & Cai, W. J. (2013). Estuarine acidification and minimum buffer zone—a conceptual study. *Geophysical Research Letters*, *40*(19), 5176-5181. https://doi.org/10.1002/grl.51000

Ianson, D., Allen, S. E., Moore-Maley, B. L., Johannessen, S. C., & Macdonald, A. R. W. (2016). Vulnerability of a semienclosed estuarine sea to ocean acidification in contrast with hypoxia. *Geophysical Research Letters*, *43*(11), 5793-5801. https://doi.org/10.1002/2016GL068996

Jartun, M., Ottesen, R. T., Steinnes, E., & Volden, T. (2008). Runoff of particle bound pollutants from urban impervious surfaces studied by analysis of sediments from stormwater traps. Science of the Total Environment, 396(2-3), 147-163. doi:10.1016/j.scitotenv.2008.02.002

Jewett, E. B., E. B. Osborne, K. M. Arzayus, K. Osgood, B. J. DeAngelo, J. M. Mintz. Eds., 2020: NOAA Ocean, Coastal, and Great Lakes Acidification Research Plan: 2020-2029, https://oceanacidification.noaa.gov/ResearchPlan2020

Jiang, L.-Q., R. A. Feely, B. R. Carter, D. J. Greeley, D. K. Gledhill, and K. M. Arzayus (2015), Climatological distribution of aragonite saturation state in the global oceans, Global Biogeochem. Cycles, 29, 1656–1673, doi:10.1002/2015GB005198.

Jiang, Z. P., Tyrrell, T., Hydes, D. J., Dai, M., & Hartman, S. E. (2014). Variability of alkalinity and the alkalinity-salinity relationship in the tropical and subtropical surface ocean. Global Biogeochemical Cycles, 28(7), 729-742.

Keller, K. M., Joos, F., and Raible, C. C.: Time of emergence of trends in ocean biogeochemistry, Biogeosciences, 11, 3647–3659, https://doi.org/10.5194/bg-11-3647-2014, 2014.

Kerr, D. E., Brown, P. J., Grey, A., & Kelleher, B. P. (2021). The influence of organic alkalinity on the carbonate system in coastal waters. Marine Chemistry, 237, 104050.

Ko, Y.H., Lee, K., Eom, K.H. and Han, I.-S. (2016), Organic alkalinity produced by phytoplankton and its effect on the computation of ocean carbon parameters. Limnol. Oceanogr., 61: 1462-1471. https://doi.org/10.1002/lno.10309

Kortazar, L., Milea, D., Gómez-Laserna, O., & Fernández, L. A. (2019). Accurate determination of total alkalinity in estuarine waters for acidification studies. TrAC Trends in Analytical Chemistry, 114, 69-80.

Kuliński, K., Schneider, B., Hammer, K., Machulik, U., & Schulz-Bull, D. (2014). The influence of dissolved organic matter on the acid–base system of the Baltic Sea. Journal of Marine Systems, 132, 106-115.

LBHMC (2021) Long Bay Hypoxia Monitoring Consortium

Lee, K., Kim, T. W., Byrne, R. H., Millero, F. J., Feely, R. A., & Liu, Y. M. (2010). The universal ratio of boron to chlorinity for the North Pacific and North Atlantic oceans. Geochimica et Cosmochimica Acta, 74(6), 1801-1811.

Lewis, E., Wallace, D. W. R., & Allison, L. J. (1998). Program developed for CO2 system calculations, carbon dioxide information analysis center. *Oak Ridge National Laboratory, Oak Ridge, Tenn*. https://doi.org/10.2172/639712

Libes, Susan; Young, Heather; Newquist, Daniel; and Sledz, Sue (2015) "Watershed-Based Planning for Murrells Inlet: Source Assessment of Fecal Bacteria Using Volunteer and Shellfish Sanitation Program Data," Journal of South Carolina Water Resources: Vol. 2 : Iss. 1 , Article 5. https://doi.org/10.34068/JSCWR.02.05

Lueker, T. J., Dickson, A. G., & Keeling, C. D. (2000). Ocean pCO2 calculated from dissolved inorganic carbon, alkalinity, and equations for K1 and K2: validation based on laboratory measurements of CO2 in gas and seawater at equilibrium. Marine chemistry, 70(1-3), 105-119.

Mallin, M. A., Burkholder, J. M., Cahoon, L. B., & Posey, M. H. (2000). North and South Carolina coasts. Marine Pollution Bulletin, 41(1-6), 56-75

McGuirk Flynn. (2008). Organic Matter and Nutrient Cycling in a Coastal Plain Estuary: Carbon, Nitrogen, and Phosphorus Distributions, Budgets, and Fluxes. Journal of Coastal Research, 10055(10055), 76–94. https://doi.org/10.2112/SI55-010.1

Melzner, F., Thomsen, J., Koeve, W., Oschlies, A., Gutowska, M. A., Bange, H. W., Hansen, H., Körtzinger, A. (2013). Future ocean acidification will be amplified by hypoxia in coastal habitats. Marine Biology, 160, 1875-1888.

Muehllehner, N., C. Langdon, A. Venti, and D. Kadko (2016), Dynamics of carbonate chemistry, production, and calcification of the Florida Reef Tract (2009–2010): Evidence for seasonal dissolution, Global Biogeochem. Cycles, 30, 661–688, doi:10.1002/2015GB005327.

Millero, F. J., Lee, K., & Roche, M. (1998). Distribution of alkalinity in the surface waters of the major oceans. Marine Chemistry, 60(1-2), 111-130.

Müller, J. D., Schneider, B., & Rehder, G. (2016). Long-term alkalinity trends in the Baltic Sea and their implications for CO2-induced acidification. *Limnology and Oceanography*, *61*(6), 1984-2002. https://doi.org/10.1002/lno.10349

Myrtle Beach Fishing (April 5, 2024 Update). (n.d.). https://fishingstatus.com/fishing/destination/myrtlebeach#:~:text=Myrtle%20Beach%20may%20be%20known,14%20million%20visitors%20per%20year.

Patsavas, M. C., Byrne, R. H., Wanninkhof, R., Feely, R. A., & Cai, W. J. (2015). Internal consistency of marine carbonate system measurements and assessments of aragonite saturation state: Insights from two US coastal cruises. *Marine Chemistry*, *176*, 9-20. https://doi.org/10.1016/j.marchem.2015.06.022

Perez, F. F., & Fraga, F. (1987). Association constant of fluoride and hydrogen ions in seawater. Marine Chemistry, 21(2), 161-168.

Pierrot, D., Epitalon, J.-M., Orr, J. C., Lewis, E., and Wallace, D. W. R. (2021) MS Excel program developed for CO2 system calculations – version 3.0, GitHub repository. Available at: https://github.com/dpierrot/co2sys_xl.

Pimenta, A. R., & Grear, J. S. (2018). Guidelines for Measuring Changes in Seawater pH and Associated Carbonate Chemistry in Coastal Environments of the Eastern United States.

Redfield, A. C. (1963). The influence of organisms on the composition of seawater. *The sea*, *2*, 26-77.

Revicki, D. (2014). Internal Consistency Reliability. In: Michalos, A.C. (eds) Encyclopedia of Quality of Life and Well-Being Research. Springer, Dordrecht. https://doi.org/10.1007/978-94-007-0753-5_1494

Reimer, Janet J. et al. (2017). Time series pCO2 at a coastal mooring: Internal consistency, seasonal cycles, and interannual variability. 145https://doi.org/https://doi.org/10.1016/j.csr.2017.06.022

Rockström, J., Steffen, W., Noone, K., Persson, Å., Chapin III, F. S., Lambin, E., ... & Foley, J. (2009). Planetary boundaries: exploring the safe operating space for humanity. Ecology and society, 14(2).

Robbins, L. L., Daly, K. L., Barbero, L., Wanninkhof, R., He, R., Zong, H., et al. (2018). Spatial and temporal variability of pCO2, carbon fluxes, and saturation state on

the West Florida Shelf. Journal of Geophysical Research: Oceans, 123, 6174–6188. https://doi.org/10.1029/2018JC014195

Sabine, C. L., Feely, R. A., Gruber, N., Key, R. M., Lee, K., Bullister, J. L., et al. (2004). The oceanic sink for anthropogenic CO2. Science 305, 367–371. doi: 10.1126/science.1097403

Salisbury, J., Green, M., Hunt, C., & Campbell, J. (2008). Coastal acidification by rivers: a threat to shellfish?. Eos, Transactions American Geophysical Union, 89(50), 513-513.

Sanger D, Hernandez D, Libes S, Voulgaris G, Davis B, Smith E, Shuford R, Porter D, Koepfler E, Bennett J. A case history of the science and management collaboration in understanding hypoxia events in Long Bay, South Carolina, USA. Environ Manage. 2010 Sep;46(3):340-50. doi: 10.1007/s00267-010-9529-8. Epub 2010 Jul 31. PMID: 20676889.

Sanger, Denise & Smith, Erik & Voulgaris, George & Koepfler, Erik & Libes, Susan & Riekerk, George & Bergquist, Derk & Greenfield, Dianne & Wren, Ashley & Mccoy, Clayton & Viso, Richard & Peterson, R. & Whitaker, J. (2012). Constrained enrichment contributes to hypoxia formation in Long Bay, South Carolina (USA), an open water urbanized coastline. Marine Ecology Progress Series. 461. 15-30. 10.3354/meps09796.

Schulz, K. G., & Riebesell, U. (2013). Diurnal changes in seawater carbonate chemistry speciation at increasing atmospheric carbon dioxide. Marine Biology, 160, 1889-1899.

Schwieterman, G. D., Crear, D. P., Anderson, B. N., Lavoie, D. R., Sulikowski, J. A., Bushnell, P. G., & Brill, R. W. (2019). Combined effects of acute temperature change and elevated p CO2 on the metabolic rates and hypoxia tolerances of clearnose skate (Rostaraja eglanteria), summer flounder (Paralichthys dentatus), and thorny skate (Amblyraja radiata). Biology, 8(3), 56.

Simone, M. N., Schulz, K. G., Oakes, J. M., & Eyre, B. D. (2021). Warming and ocean acidification may decrease estuarine dissolved organic carbon export to the ocean. *Biogeosciences*, *18*(5), 1823-1838. https://doi.org/10.5194/bg-18-1823-2021

Soetaert, K., Hofmann, A. F., Middelburg, J. J., Meysman, F. J., & Greenwood, J. (2007). Reprint of "The effect of biogeochemical processes on pH". *Marine Chemistry*, *106*(1-2), 380-401. https://doi.org/10.1016/j.marchem.2007.06.008

Solomon, S., Qin, D., Manning, M., Alley, R. B., Berntsen, T., Bindoff, N. L., Wratt, D. (2007). Technical summary. Climate Change 2007: The Physical Science Basis. Contribution of Working Group I to the Fourth Assessment Report of the Intergovernmental Panel on Climate Change [Solomon, S., D. Qin, M. Manning, Z. Chen, M. Marquis, KB Averyt, M. Tignor and HL Miller (eds.)].Sutton, Adrienne J. et al. (2019). Autonomous seawater pCO2 and pH time series from 40 surface buoys and the emergence of anthropogenic trends. 11(1). https://doi.org/10.5194/essd-11-421-2019

Suzuki, A., & Kawahata, H. (2003). Carbon budget of coral reef systems: an overview of observations in fringing reefs, barrier reefs and atolls in the Indo-Pacific regions. Tellus B: Chemical and Physical Meteorology, 55(2), 428-444.

Tanhua, T., Orr, J. C., Lorenzoni, L., & Hansson, L. (2015). Monitoring ocean carbon and ocean acidification. Bulletin nº, 64, 1.

Talmage SC, Gobler CJ (2011) Effects of elevated temperature and carbon dioxide on the growth and survival of larvae and juveniles of three species of Northwest Atlantic bivalves. PLoS One 6: e26941.

Talmage SC, Gobler CJ (2012) Effects of CO2 and the harmful alga Aureococcus anophagefferens on growth and survival of oyster and scallop larvae. Mar Ecol Prog Ser 464: 121–134

The MathWorks Inc. (2023). MATLAB version: 9.14.0 (R2023a), Natick, Massachusetts: The MathWorks Inc. https://www.mathworks.com

Troup, M. L., Fribance, D. B., Libes, S. M., Gurka, R., & Hackett, E. E. (2017). Physical conditions of coastal hypoxia in the open embayment of Long Bay, South Carolina: 2006–2014. *Estuaries and Coasts*, *40*(6), 1576-1591. https://doi.org/10.1007/s12237-017-0246-x

Viso, R., McCoy, C., Gayes, P., & Quafisi, D. (2010). Geological controls on submarine groundwater discharge in Long Bay, South Carolina (USA). Continental Shelf Research, 30(3-4), 335-341.

Wallace, R. B., Baumann, H., Grear, J. S., Aller, R. C., & Gobler, C. J. (2014). Coastal ocean acidification: The other eutrophication problem. Estuarine, Coastal and Shelf Science, 148, 1-13.

Wang, Z. A., & Cai, W. J. (2004). Carbon dioxide degassing and inorganic carbon export from a marsh-dominated estuary (the Duplin River): A marsh CO2 pump. *Limnology and Oceanography*, *49*(2), 341-354. https://doi.org/10.4319/lo.2004.49.2.0341

Wang, Z. A., Kroeger, K. D., Ganju, N. K., Gonneea, M. E., & Chu, S. N. (2016). Intertidal salt marshes as an important source of inorganic carbon to the coastal ocean. Limnology and Oceanography, 61(5), 1916-1931.

Wanninkhof, R., Barbero, L., Byrne, R., Cai, W. J., Huang, W. J., Zhang, J. Z., Baringer, M., & Langdon, C. (2015). Ocean acidification along the Gulf Coast and East Coast of the USA. *Continental Shelf Research*, *98*, 54-71. https://doi.org/10.1016/j.csr.2015.02.008

WWA (2021) Volunteer Water Monitoring Program: Murrells Inlet

Xia, M., Xie, L., & Pietrafesa, L. J. (2007). Modeling of the Cape Fear River estuary plume. Estuaries and Coasts, 30, 698-709.

Xue, L., Cai, W. J., Hu, X., Sabine, C., Jones, S., Sutton, A. J., Jiang, L., & Reimer, J. J. (2016). Sea surface carbon dioxide at the Georgia time series site (2006–

2007): Air–sea flux and controlling processes. *Progress in Oceanography*, *140*, 14-26. https://doi.org/10.1016/j.pocean.2015.09.008

Yang, B., Byrne, R. H., & Lindemuth, M. (2015). Contributions of organic alkalinity to total alkalinity in coastal waters: A spectrophotometric approach. Marine Chemistry, 176, 199-207.